Neurobiology of Disease 127 (2019) 264–277

Contents lists available at ScienceDirect

Neurobiology of Disease

journal homepage: www.elsevier.com/locate/ynbdi

Regional hypometabolism in the 3xTg mouse model of Alzheimer's disease

Aida Adlimoghaddam[a,b,*], Wanda M. Snow[a], Greg Stortz[c], Claudia Perez[a,b], Jelena Djordjevic[a,b], Andrew L. Goertzen[d], Ji Hyun Ko[e,f], Benedict C. Albensi[a,b,*]

[a] St. Boniface Hospital Research, Canada
[b] Dept. of Pharmacology & Therapeutics, University of Manitoba, Canada
[c] University of British Columbia, Canada.
[d] Dept. of Radiology, University of Manitoba, Canada
[e] Dept. of Human Anatomy and Cell Science, University of Manitoba, Canada
[f] Health Sciences Centre, Canada

ARTICLE INFO

Keywords:
Alzheimer's disease, 3xTg-AD, neurofibrillary tangles
Amyloid beta
FDG-PET
Insular
Pirifom

ABSTRACT

Alzheimer's disease (AD) is a progressive age-related neurodegenerative disease. Although neurofibrillary tangles and amyloid beta are classic hallmarks of AD, the earliest deficits in AD progression may be caused by unknown factors. One suspected factor has to do with brain energy metabolism. To investigate this factor, brain metabolic activity in 3xTg-AD mice and age-matched controls were measured with FDG-PET. Significant hypometabolic changes ($p < .01$) in brain metabolism were detected in the cortical piriform and insular regions of AD brains relative to controls. These regions are associated with olfaction, which is a potential clinical marker for AD progression as well as neurogenesis. The activity of the terminal component of the mitochondrial respiratory chain (complex IV) and the expression of complex I-V were significantly decreased ($p < .05$), suggesting that impaired metabolic activity coupled with impaired oxidative phosphorylation leads to decreased mitochondrial bioenergetics and subsequent Neurodegeneration. Although there is an association between neuroinflammatory pathological markers (microglial) and hypometabolism in AD, there was no association found between neuropathological (Aβ, tau, and astrocytes) and functional changes in AD sensitive brain regions, also suggesting that brain hypometabolism occurs prior to AD pathology. Therefore, targeting metabolic mechanisms in cortical *piriform* and *insular* regions at early stages may be a promising approach for preventing, slowing, and/or blocking the onset of AD and preserving neurogenesis.

1. Introduction

Alzheimer's disease (AD) is a progressive age-related neurodegenerative disorder characterized by cognitive impairment (McKeith and Cummings, 2005). Neuropathologically, AD is defined by the accumulation of senile plaques, largely composed of extracellular deposits of amyloid B (Aβ) peptide, and neurofibrillary tangles (NFTs), composed of intracellular filamentous aggregates of hyperphosphorylated tau protein (Glabe, 2005; Hardy and Selkoe, 2002). Deposition of Aβ plaques and NFTs are well-established hallmarks of AD, leading to synapse loss and neuronal death (Ellis et al., 1996; Price et al., 2001). However, it has also been shown that AD pathology begins > 10 years prior to any of the clinical symptoms of the disease become apparent (Braak and Braak, 1996; Delacourte et al., 1999; Ellis et al., 1996). Interestingly, some clinical studies have found pathological lesions in subjects with and without diagnosed AD at the time of autopsy (Braak and Braak, 1991; Delacourte et al., 1999; Ellis et al., 1996). As highlighted by a clinical autopsy study investigating nearly 1000 cases, 30% of clinically diagnosed AD cases lacked the presence of postmortem Aβ plaques. The study also highlighted that 40% of cases clinically recognized as non-AD cases display accumulation of Aβ plaques (Beach et al., 2012). This result suggests that Aβ plaques alone cannot be used to accurately confirm and diagnose AD during early stages, and thus additional factors are involved warranting investigation (Beach et al., 2012).

Overall, most investigators consider AD to be a multifactorial neurodegenerative disorder. In fact, an emerging view is that the earliest deficits in the pathological progression of AD are associated with impaired energy metabolism (Blass et al., 2000; Mosconi et al., 2008a; Parihar and Brewer, 2007; Valla et al., 2001). Metabolic processing of glucose to adenosine tri-phosphate (ATP) involves three main metabolic pathways: glycolysis in the cytosol and the TCA cycle as well as oxidative phosphorylation in the mitochondria. In particular, previous

* Corresponding authors at: St. Boniface Hospital Research, Canada.
E-mail addresses: aadlimoghaddam@sbrc.ca (A. Adlimoghaddam), balbensi@sbrc.ca (B.C. Albensi).

https://doi.org/10.1016/j.nbd.2019.03.008
Received 13 July 2018; Received in revised form 22 February 2019; Accepted 12 March 2019
Available online 14 March 2019
0969-9961/

studies have shown that AD pathology is associated with aberrations in metabolic activity and/or the expression of enzymes involved in mitochondrial function (Electron Transport Complexes (ETC) and Krebs cycle (tricarboxylic acid; TCA)) (Blass et al., 2000; Bubber et al., 2005; Gibson et al., 2000; Parker Jr. et al., 1990). In addition to the lowered mitochondrial functional capacity in AD, reduction in cerebral glucose utilization is associated with reduction in the expression of glycolytic enzymes that would be expected to decrease ATP synthesis (Ishii et al., 1997). Moreover, genetic and neuroproteomic studies have shown a potential association between glycolysis and AD-associated proteins (Aβ and tau) (Butterfield et al., 2010; El Kadmiri et al., 2014; Sunaga et al., 1995). Additionally, disruption in glucose metabolism is associated with synaptic dysfunction that is correlated with later clinical impairment in AD (Duara et al., 1986; Friedland et al., 1983; Haxby et al., 1986; Perneczky et al., 2007; Sokoloff, 1981). Overall, several studies provide strong evidence that impaired brain glucose metabolism is one of the most important clinical and biochemical features leading to AD (Ballatore et al., 2007; Hansson and Gouras, 2016; Hardy and Selkoe, 2002; Marcus et al., 2014; Shokouhi et al., 2014; Small and Duff, 2008). In clinical studies, Positron Emission Tomography (PET) with 2-deoxy-2-[^{18}F]fluoroglucose ([^{18}F]FDG) has been utilized to assess cerebral metabolic rates of glucose uptake in the brain of AD patients. FDG-PET neuroimaging has also been utilized for visualizing brain activity in rodents (Baek et al., 2016; Mirrione et al., 2007; Nicholson et al., 2010). FDG-PET is a cutting-edge in vivo method for evaluating qualitative and quantitative metabolic alterations of brain at the tissue level. FDG-PET neuroimaging offers the identification of reliable biomarkers in dementia, which can help clinicians with earlier diagnosis, characterization of dementia type, and the evaluation of drug effectiveness (Duara et al., 1986; Friedland et al., 1983; Haxby et al., 1986; Sokoloff, 1981). Some FDG-PET studies suggest hypometabolism (decreased in glucose uptake) and some others detect hypermetabolism (increased in glucose uptake) in AD transgenic models. For example, hypometabolism was detected in hippocampal and cortical tissues of 2 and 3 months old APP(Tg2576) mice (Niwa et al., 2002). However, hypermetabolism was observed in cortical areas of 7, 16 and 19 months old APP(Tg2576) mice (Luo et al., 2012; Valla et al., 2006). Additionally, hypermetabolism was detected in cortical regions of 16 months old APP (Tg2576)xPS1M146L (Poisnel et al., 2012; Valla et al., 2006). In PDAPP V717F mice, cortical and hippocamplal hypermetabolism was observed at 2, 12 and 17 months of age, whereas cortical hypometabolism was detected in 3, 10 and 17 months old (Reiman et al., 2000; Valla et al., 2008). Hypermetabolism was seen in 7 months old 3xTg-AD, 10 months old 5XFAD mice and 5 months old B6.PS2APP mice (Brendel et al., 2016; Cristea et al., 2013; Sancheti et al., 2014). Inconsistent metabolic activities are depending on the age or disease progression and type of AD mouse model. Some transgenic mouse models develop a more severe phenotype and express amyloid plaques much earlier than other types. Since the pathology observed in various transgenic mouse models is different, therefore various level of glucose uptake was detected. The accumulation of amyloid is accompanied by significant increasing in numbers of microglial cells. Activated microglial cells can reduce accumulation of amyloid deposits by increasing its degradation which directly causes neuronal hyperactivity and this is a possible explanation for hypermetabolism in AD mice models (Backes et al., 2016; Brendel et al., 2016; Busche et al., 2012; Weiner and Frenkel, 2006). Therefore, level of glucose uptake in AD mice is related to the inflammatory process induced by amyloid plaques (Ashraf et al., 2015; Cristea et al., 2013; Klupp et al., 2015; Oh et al., 2016).

This inconsistency in metabolic status also has been shown in clinical studies. For example, cortical hypometabolism was detected in mild cognitive impairment (MCI) subjects with high amyloid deposition and whereas cortical hypermetabolism was observed mainly in amyloid-negative MCI subjects. Clinical follow up has been shown that MCI subjects with hypometabolism and high amyloid load converted to AD and MCI subjects with hypermetabolism and much less amyloid deposition did not convert to AD (Ashraf et al., 2015; Klupp et al., 2015; Oh et al., 2016). Accumulations of amyloid plaques activate glial cells. In particular, activated microglial cells in AD had increased glucose consumption to mediate the neuroinflammatory process in the brain and display compensatory neuronal activity (Calsolaro and Edison, 2016; Eikelenboom et al., 2002; Heneka et al., 2015; Jeong et al., 2017; Tan et al., 2002; Tan et al., 1999; Wyss-Coray, 2006). Overall, these data suggested that patients with MCI have been shown to transition from a state of hypermetabolism, during the early stages of amyloid plaque deposition, to a hypometabolism state, following significant amyloid deposition. This transition is known to occur because the brain needs to maintain balance as the neurons begin to diminish in their numbers and capacities (Ashraf et al., 2015).

The most vulnerable brain areas in AD are the medial temporal lobes (MTL, i.e., the hippocampus (subiculum region), transentorhinal and entorhinal cortices, and parahippocampal gyrus), which are typically associated with learning/memory and are most susceptible to AD pathology and hypometabolism (Arriagada et al., 1992; Braak and Braak, 1991; De Santi et al., 2001; Jack Jr. et al., 2010; Mosconi, 2005; Nestor et al., 2003; Snow et al., 2017; Ulrich, 1985). Earlier FDG-PET studies comparing patterns of brain metabolic activity between AD patients and those with mild cognitive impairment (MCI) demonstrated hypometabolism in the posterior cingulate gyrus, hippocampus and parahippocampal gyrus in the MCI group, whereas in the AD group, hypometabolism was evident in the limbic network (amygdala and temporoparietal and frontal association cortex), precuneus, inferior parietal, posterior cingulate cortex, and middle temporal lobes (Del Sole et al., 2008; Nestor et al., 2003). These studies reveal a different regional metabolic pattern between AD and MCI, a finding which, in conjunction with symptomology, may help confirm diagnoses. Moreover, the extent and topography of metabolic deficits correlates with the progression and severity of AD (Mosconi et al., 2008a). Clinical FDG–PET studies have shown that hypometabolism occurs in the posterior cingulate cortex, precuneus, parieto-temporal areas (hippocampus), and middle temporal gyrus especially at the early stages of AD, whereas in advanced disease, frontal lobes are mostly involved (Brown et al., 2014; Chetelat et al., 2008; De Santi et al., 2001; Kim et al., 2005; Minoshima et al., 1997; Silverman et al., 2001). However, metabolic activity within other regions, such as visual and anterior cingulate cortices, cerebellum, thalamic and basal ganglia and posterior fossa remain relatively spared in AD (Foster et al., 1984; Friedland et al., 1983; Minoshima et al., 1997; Morbelli et al., 2010; Mosconi, 2005; Mosconi et al., 2008b; Salmon et al., 2000; Silverman et al., 2001). In preclinical studies, transgenic mouse models showed hypometabolism in the hippocampus, amygdala, entorhinal cortex, cingulate cortex, temporal cortex, and parietal cortex (association neocortex), similar to findings obtained in patients with AD (Ashe and Zahs, 2010; Reiman et al., 2000; Valla et al., 2008; Valla et al., 2006).

To date, most neuroimaging studies have concentrated on investigating the metabolic activity in subjects in the early stage of AD; however, studies investigating the association between hypometabolism and AD pathology have been limited and are unresolved. To fill this gap, we applied FDG-PET neuroimaging to a triple transgenic AD mouse (3xTg), which exhibits several age-dependent hallmarks of AD, including amyloid plaque deposition and tau tangles, as well as memory deficits (Oddo et al., 2003b). A detailed pathological progression in this mouse model has been reported in an age-dependent manner (Mastrangelo and Bowers, 2008). Initial characterizations of the 3xTg strain demonstrated that unlike tau pathology, which appears at 9 months of age, amyloid plaques exhibit as early as 2 months of age (Mastrangelo and Bowers, 2008). In this study we choose 11 months old 3xTg mice to evaluate metabolic statues at time point that 3xTg developed both pathological hallmarks. Specifically, we: 1) used the standard uptake value (SUV) analysis of FDG-PET in AD to identify disease-specific metabolic brain patterns in male 3xTg mice relative to

age-matched controls; 2) compared the levels of key enzymes involved in metabolic pathways (glycolysis, TCA, and ETC) between 3xTg mice and their control group; and 3) investigated if Aβ and tau pathology is temporally and regionally associated with metabolic activity. Using this approach, we found that region-specific brain hypometabolism is unrelated to amyloid plaque and tangle deposition.

2. Materials and methods

2.1. Animals

In our study, we used the 3xTg strain, which was originally a gift from Dr. Mark Mattson (NIH, Baltimore, Maryland). These mice were maintained on a C57BL/6 background for over eight generations. Homozygous 3xTg mice were bred and housed at St. Boniface Hospital Research. These transgenic mice harboring the APP_{Swe}, $PS1_{M146V}$, and Tau_{P301L} mutations exhibit Aβ and tau pathology and synaptic dysfunction. The background strain for the 3xTg colonies, C57BL/6, served as controls. A total of 10 ($n = 5$ per group) 3xTg mice, a transgenic model of AD, and age-matched control C57BL/6 male mice underwent PET scanning at 11 months of age. These methods were approved by the University of Manitoba animal care and use committee, which adheres to guidelines set forth by the Canadian Council on Animal Care. This work complies with the ARRIVE guidelines. Both 3xTg and control mice were aged at St. Boniface Hospital Research. Mice were housed in the pathogen-free animal facility at St. Boniface Research Centre. Mice were given ad libitum access to food and water and maintained under the standard light/dark cycle (12 h light, 12 h dark).

2.2. PET

2.2.1. PET acquisition

Food was withheld from the mice for 6 h prior to the PET imaging studies. Thirty minutes prior to injection, the mouse cage was placed on a warming pad maintained at 37 °C. For injection, the mouse was briefly anaesthetized using isoflurane and then injected i.p. with 5.5 ± 1.1 MBq ^{18}F-FDG in a total volume < 0.2 ml. The mouse was then returned to its cage on the warming pad for the tracer uptake period. Fifty minutes post-injection the mouse was anaesthetized using isoflurane and placed into a custom mouse bed that supplied anesthetic gas and incorporated a quadrature surface coil for brain imaging. Simultaneous PET/MR imaging was performed for 20 min starting 60 min post-injection using a custom built MR compatible PET insert operating inside a 7 T Bruker Avance III MRI system (Bruker Corporation, Billerica, MA) equipped with a BGA-12S gradient coil. The PET insert has an axial field of view (FOV) of 28.1 mm and clear bore diameter of 60.3 mm, with spatial resolution < 1.86 mm over the central 30 mm diameter of the field of view (FOV) (Goertzen et al., 2015; Stortz et al., 2017; Thiessen et al., 2016). PET images were reconstructed using a point spread function (PSF) modeling maximum likelihood method (PSF-MLEM) using an isotropic voxel size of 0.635 mm (Zhang et al., 2013). MR data were acquired using a half-Fourier acquisition-single-shot-turbo-spin-echo (HASTE) sequence with in-plane resolution of 0.15875 mm. Additional details on the PET system can be found in Stortz et al. (Stortz et al., 2017).

2.2.2. PET analysis

An in-house FDG-PET template was created using two additional adult wild-type mice; the FDG-PET images of which were paired with the simultaneously acquired T2-weighted MRI. The T2-MRI images were spatially normalized after segmentation (Ashburner and Friston, 2000, 2005) to the standard T2-MRI template for adult control (C57BL/6) mice (Ma et al., 2005). The same spatial transformation matrices were used to spatially normalize the FDG-PET images and then averaged to produce the in-house FDG-PET template using coordinates as per Paxinos(Paxinos and Franklin, 2013).

All FDG-PET images were spatially normalized to the in-house FDG-PET template, then smoothed with a Gaussian filter (FWHM: 0.4 × 0.4 × 0.4 mm). The SUVs were calculated for each voxel. All preprocessing and imaging analysis were performed using default parameters of.

SPMMouse software (http://www.spmmouse.org) running on SPM5 (www.fil.ion.ucl.ac.uk/spm/software/spm5/). The clusters (extent threshold: ke > 100) with peak threshold ($p < .01$, uncorrected) were considered significant.

2.2.3. Brain tissue collection

After FDG-PET imaging, cortical piriform and insular tissue was extracted from the brains of same mice that underwent imaging after euthanasia by decapitation while under isoflurane anesthetic. After PET imaging, all western blotting and enzyme assay procedures were carried out using half brains allowing the remaining tissue to be used for other experiments (immunohistochemistry and congo red staining), and thereby reduce the number of animals used.

2.2.4. Preparation of isolated mitochondria from brain

Mitochondria from piriform and insular cortex, in which glucose metabolism was altered, were isolated from control and AD mice (C57BL/6 and 3xTg) that underwent FDG-PET imaging. Mitochondria were isolated using the commercial isolation kit (8268, ScienCell Research Laboratory, Carlsbad, California, USA) as reported previously (Trounce et al., 1996). Briefly, brain tissues were washed twice with PBS and then homogenized in isolation buffer. Homogenates were centrifuged at 1000 ×g for 5 min at 4 °C. Supernatants were further centrifuged at 10,000 ×g for 20 min at 4 °C. Resultant pellets were used as mitochondrial fractions, and supernatants were used as cytosolic fractions. Further, the protein concentrations of the enriched mitochondrial fractions were measured using a colorometric DC protein assay kit (BioRad, Hercules, California, USA).

2.3. Enzyme activities

2.3.1. Measurement of GAPDH enzymatic activity

Enzymatic activity of Glyceraldehyde 3-Phosphate Dehydrogenase (GAPDH) was measured in cortical cytosolic fraction by the GAPDH Activity Colorimetric Assay Kit (ab204732, Abcam, Cambridge, Massachusetts, USA). The measurement of GAPDH activity, based on the conversion of NAD^+ to NADH, was accomplished by tracking the change of absorbance at 450 nm for two minutes at 37 °C using a spectrophotometer MRX Micoplate Reader (Dynex Technologies, Denkendorf, Germany). The specific GAPDH activity was determined as units per milligram of protein, where 1 unit is defined as the amount of enzyme producing 1 μmol of NADH/min.

2.3.2. Measurement of cytochrome C oxidase and citrate synthase enzymatic activity

The activity of mitochondrial cytochrome *c* oxidase (COX) and citrate synthase (CS) was assessed spectrophotometrically (Ultrospec 2100 pro; GE Healthcare) using ScienCell assay kits (8278 and 8318, ScienCell Research Laboratory, California, USA) in isolated cortical mitochondrial preparations. The activity of COX was determined by measuring the oxidation of reduced cytochrome *c* at 550 nm. The activity of CS was measured as the difference in the rate of absorbance (412 nm) in the presence and absence of 1.0 mmol L^{-1} oxaloacetate.

2.3.3. Protein extraction and Western blotting

Brain tissue from piriform and insular cortex of control and AD mice that underwent FDG-PET imaging were homogenized in RIPA buffer consisting of: 50 mM Tris, pH 8.0, 150 mM sodium chloride, 0.1% sodium dodecyl sulfate (SDS), 0.5% sodium deoxycholate, 1% Triton X-100, 1% phosphatase inhibitor cocktail (Sigma-Aldrich, St. Louis, MO, USA), and 1% protease inhibitor cocktail (Amresco, Solon, OH, USA).

Further, homogenates were centrifuged at 10,000 ×*g* for 10 min at 4 °C, the supernatants were collected, and the protein concentration was quantified using the bicinchoninic (BCA) assay. Further, all samples were treated with 4× laemmli buffer (16% SDS, 20% β-mercaptoethanol, 0.01% bromophenol blue, 40% glycerol, and 0.25 M Tris, pH 6.8), and heated for eight minutes at 40 °C. Protein concentrations were measured using a colorometric DC protein assay kit (BioRad, Hercules, California, USA). Equivalent amounts of protein (20 μg) from each sample were loaded and subjected to SDS-PAGE at 180 V in polyacrylamide gels (Bio-Rad, Hercules, California, USA). Following electrophoresis, gels were activated utilizing a ChemiDoc imager (Bio Rad, Hercules, California, USA). Afterwards, proteins were transferred from gels into the nitrocellulose membranes (Bio-Rad, Hercules, California, USA) utilizing the Trans-Blot Turbo Transfer System (Bio-Rad, Hercules, California, USA). Following successful transfer, total proteins on the membranes were measured utilizing the ChemiDoc imager. After imaging, the membranes were incubated for one hour at room temperature on a teetering platform in TBS-T buffer with 5% milk. All membranes were then incubated overnight at 4 °C with the following primary antibodies: Total OXPHOS Rodent WB Antibody Cocktail (ab110413, Abcam, Cambridge, Massachusetts, USA, 1:1000 dilution). The following day, membranes were washed with 1× TBS-T buffer (three times; 10 min each). All membranes were then incubated with goat anti-mouse IgG (H + L) antibody (Jackson ImmunoResearch Laboratories, West Grove, PA, USA, 1:2000 dilution) prepared in TBS-T buffer with 5% milk for one and half hours at 4 °C. Later, membranes were washed with 1× TBS-T buffer (three times; 10 min each). The membranes were treated with enhanced chemiluminescence (ECL) using Bio-Rad Clarity Weston ECL blotting kit (Bio-Rad, Hercules, California, USA), and visualized by the ChemiDoc. Relative quantification of OXPHOS protein levels was normalized to total protein.

2.4. Neuropathological staining

2.4.1. Amyloid plaque staining with congo red

Congo red staining was utilized to detect extracellular Aβ deposits in mice that underwent FDG-PET imaging. After PET scanning, brains of AD and control mice were collected after decapitation under isoflurane anesthetic. Brain tissues were fixed in paraformaldehyde for 24 h before sucrose cryoprotection and cut into 10-μm-thick horizontal sections using a cryostat, air-dried (room temperature), and stored at −80 °C until further use. As previously described, congo red staining was performed to determine the presence of amyloid deposits indicative of a neurodegenerative process (Bohnen and Jahn, 2013; Catafau and Bullich, 2015; Snow et al., 2017). Briefly, horizontal sections were rehydrated in phosphate-buffered saline (PBS, pH 7.4), for five minutes. The sections were then counterstained in Mayer's hematoxylin for three minutes followed by rinsing in running tap water for five minutes. Sections were pretreated in an alkaline alcoholic-saturated sodium chloride solution for 20 min, followed by immersion in alkaline alcoholic congo red solution for 20 min (HT60, Sigma-Aldrich). All sections were then dehydrated in absolute ethanol, cleared with Xylene (two times; five minutes each), and cover slipped with Permount mounting medium (Fisher Scientific, Waltham, MA, USA).

2.4.2. Immunohistochemistry

Immunohistochemistry was used to detect different epitopes of phospho-tau (Thr 231, Ser 202/Thr 205) deposition, intracellular Aβ plaques, and astrocytes in 3xTg and control mice that underwent FDG-PET imaging. Formation of neurofibrillary tangle, intracellular Aβ and astrocytes was assessed with immunohistochemistry as described previously (Harry et al., 2014; Hernandez-Zimbron et al., 2017; Snow et al., 2017). Briefly, the sections were rehydrated by immersion in Tris-buffered saline with 0.1% Tween 20 (TBS-T) for five minutes. Following rehydration, antigen retrieval was performed for 30 min in preheated (80 °C) citrate buffer (Tris/EDTA pH 9.0, sodium citrate pH 6.0) using a water bath. All sections were then treated with rabbit monoclonal anti-Aβ42 antibody (ab201060, abcam, Cambridge, Massachusetts, USA, 1:100 dilution) to detect soluble fibrillar aggregation-selective epitope of Aβ42 (Hatami et al., 2014) or were treated with AT180 mouse monoclonal antibody (MN1040 or MN1020 ThermoScientific, Rockford, IL, USA, 1: 100 dilution) to detect phospho-tau Thr 231 or Ser 202/Thr 205 epitopes respectively or were treated with anti-GFAP antibody (ab16997, abcam Cambridge, Massachusetts, USA, 1:100 dilution) to detect astrocytes combined with the EXPOSE mouse specific horseradish peroxidase/3–3- diaminobenzidine chromogen solution (HRP/DAB) detection immunohistochemistry kit (ab80436, Abcam, Cambridge, Massachusetts, USA). Negative controls were obtained by omission of the primary antibody. Histopathological sections were viewed with an inverted microscope (Nikon, Eclipse, TE200-U). Images captured with an infinity 2–1R CCD camera (Lumenera Corp., Ottawa, Ontario, Canada).

2.4.3. Immunofluorescence

Immunofluorescence was used to detect microglial cells in 3xTg and control mice that underwent FDG-PET imaging. Briefly, sections were rehydrated with TBS-T, followed by blocking in TBS with 10% normal goat serum for 1 h at room temperature. Immunostaining was performed with rabbit polyclonal Iba-1 (019–19,741, wako, Saitama, Japan, 1:100 dilution) to detect microglial. Primary antibodies were diluted with TBS and 10% normal goat serum and incubated overnight at 4 °C. Slides were washed and incubated for 2 h at room temperature with a goat anti-rabbit 488 secondary antibody (1:200; Invitrogen, Carlsbad, CA) to detect Iba1-stained cells. Further, slides were washed three times with TBS-T and were mounted using mounting medium with DAPI. Positively stained Iba-1 expressing cells were visualized using Carl Zeiss Axioscope-2 upright fluorescence microscope equipped with AxioVision3 software. The fluorescent signal was collected as total pixel area for microglia cells. Volume density of Iba-1 immunofluorescence was quantified using ImageJ software (http://rsbweb.nih.gov/ij/).

2.5. Statistical analysis

For analysis of enzymatic changes and Western blotting data, standard two-tailed Student's *t*-tests, were performed as appropriate (GraphPad Prism 6, GraphPad Software) to evaluate the statistical significance of differences between study groups. A $p < .05$ was considered statistically significant. Voxel-wise t-test has been used for PET analysis, in which case differences between groups were considered statistically significant at $p < .01$.

3. Results

3.1. Metabolic pattern in AD vs. control

Body weights of mice (37.54 ± 1.98 g; mean ± SD) were not significantly different between AD and control groups. The whole brain SUV values (control: 1.581 ± 0.158; AD: 1.359 ± 0.461) were not significantly different between the groups ($t(8) = 1.290$, $p = .4$). Voxel-wise t-test revealed significantly ($p < .01$) reduced FDG uptake (SUV) in the piriform area and insular cortex in AD mice vs. control mice (right peak coordinates: x = 4.0 y = 0.2 z = −4.5 mm, $k_e = 769$ and left peak coordinates: x = −4.5 y = −0.9 z = −4.1 mm, $k_e = 666$) (Table. 1; Fig. 1).

3.2. Measurement of enzymatic activity of COX, CS, and GAPDH

After FDG-PET imaging, isolated mitochondria from cortex of control and AD mice were utilized for enzymatic assays. Deregulation of glucose metabolism was evaluated by comparing the enzymatic activity of key enzymes of the glycolysis (GAPDH), tricarboxylic acid (TCA)

Table 1
Peak coordinates of lower FDG uptake in AD mice compared to the control mice.

Regions	k_E	T	P	X	Y	Z
Piriform area / insula	769	5.25	< 0.001	4.0	0.2	−4.5
		4.93	0.001	4.1	−0.7	−4.7
		4.01	0.002	2.7	0.7	−5.0
Piriform area / insula	666	4.12	0.002	−4.5	−0.9	−4.1
		3.86	0.002	−3.2	0.5	−4.5
		3.63	0.003	−3.4	0.5	−5.2

This table summarizes the clusters (k_E) > 100 with voxels that are significant lower in AD mice compared to controls at $p < .01$ (uncorrected at voxel level). No regions with significantly higher uptake in AD mice were reported.

cycle (CS), as well as ETC (COX) between AD and controls. Activity of cytochrome *c* oxidase from AD groups was significantly (t (30) = 5.377, $p = .0001$) decreased compared to that of controls (Fig. 2A). However, activity of CS (t (18) = 0.4614, $p = .6501$) and GAPDH (t (8) = 0.7287, $p = .4870$) were not significantly altered between AD and their control groups (Fig. 2B, Fig. 2C).

3.2.1. Western blot analysis

Cortical tissue was extracted for Western blot experiments to detect mitochondrial protein levels in AD mice compared to levels in controls. Based on data normalized to total protein, Western blot results revealed significantly decreased protein levels of NADH dehydrogenase beta subcomplex subunit 8 of Complex I (t (8) = 3.068, $p = .0154$), succinate dehydrogenase subunit B of Complex II (t (8) = 9.727, $p < .0001$), cytochrome *b*-c1 complex subunit 2 of Complex III (t (8) = 4.777, $p = .0014$), cytochrome *c* oxidase subunit 1 of Complex IV (t (8) = 5.674, $p = .0005$), and ATP synthase subunit alpha of Complex V (t (8) = 4.645, $p = .0017$) in AD compared to controls. All relative quantification for mitochondrial proteins (Complex 1-V) from AD mice and their control were analyzed based on densitometry values normalized to total protein level (Fig. 3A and B).

3.2.2. AD pathology

No congophilic plaques were identified in any brain region of either 3xTg or control mice (Fig. 4A, B). Evidence of Aβ plaque deposition, however, was found in sections from the cortex of 14-month-old 3xTg mice, which served as positive controls (Fig. 4C). Immunohistochemistry staining did not indicate Aβ deposits in the cortical insular and piriform of control or 3xTg mice (Fig. 4D, E). However, positive Aβ staining were detected in the entorhinal cortex of 3xTg mice but not control mice (Fig. 4F). Immunohistochemistry for hyperphosphorylated tau ((Thr 231, Ser202/Thr205), was not detected tau-positive neurons in the cortical insular and piriform of control or 3xTg mice (Fig. 5A, B), although immunoreactivity was high in the hippocampus of positive control sections from AD mice at 14-months old (Fig. 5C). Relative to the lack of tau tangles in AD in sensitive brain regions, tau-positive neurons in AD were detected in the entorhinal

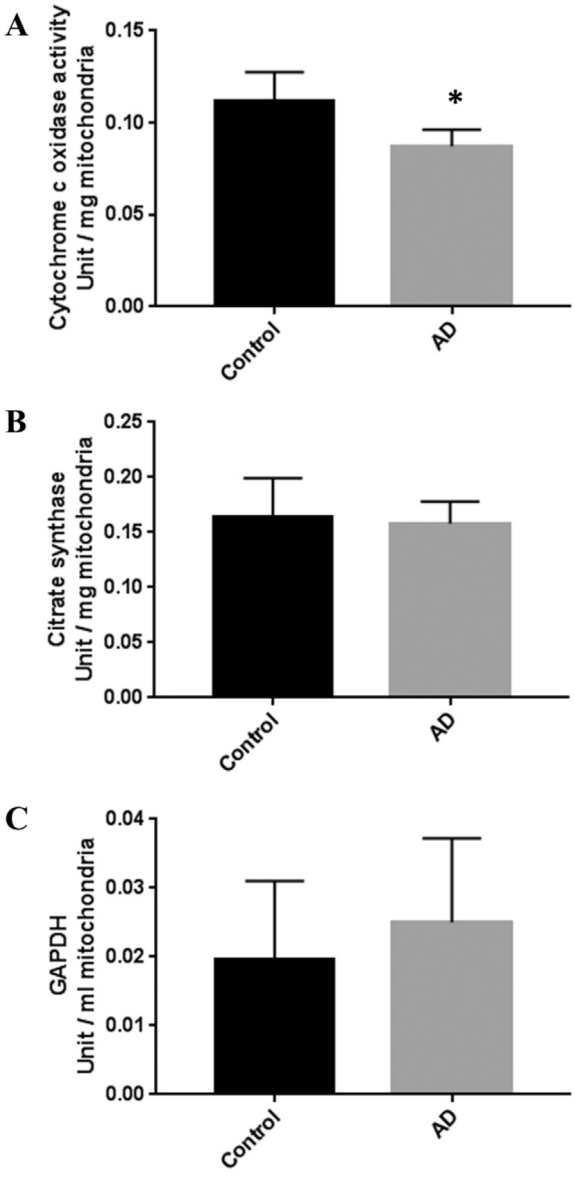

Fig. 2. Specific enzyme activities of cytochrome *c* oxidase (A; n = 5), citrate synthase (B; n = 5), and Glyceraldehyde 3-Phosphate Dehydrogenase (C; n = 5) in AD and control mice. Enzyme activities were measured spectrophotometrically from homogenates isolated from cortical piriform and insular of AD and control mice. The statistical significance is represented by asterisks (*$p < .05$) versus corresponding control group. Data represent means ± SD.

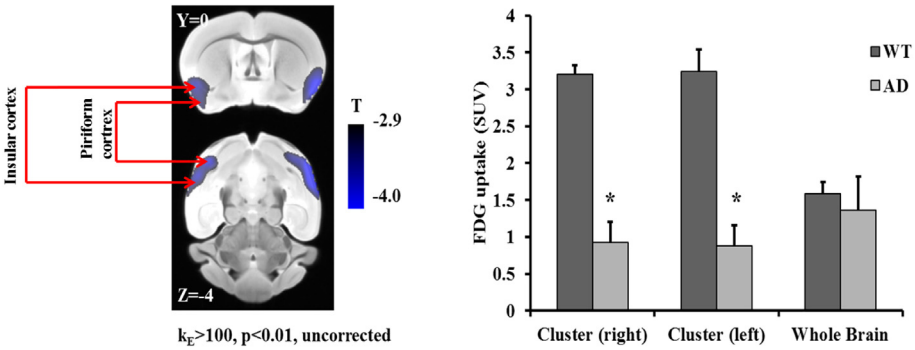

Fig. 1. Standardized uptake value (SUV) of the right and left clusters (the lump of many voxels that are significant) as well as whole brain after injection of FDG in AD and control mice. Statistical parametric mapping analysis (Two sample *T*-Test) on the regional FDG uptake. Decreased FDG uptake was observed in the bilateral piriform area and insula (labeled regions) in AD mice compared to control mice. Figure shows clusters change with extent threshold (K_E) > 100, $p < .01$ (uncorrected for multiple comparisons). The T-map is overlaid on the template MRI [118]. Results are expressed as mean ± SD of 11-month-old male AD mice ($n = 5$) and age-matched controls (n = 5) male mice (*$p < .01$).

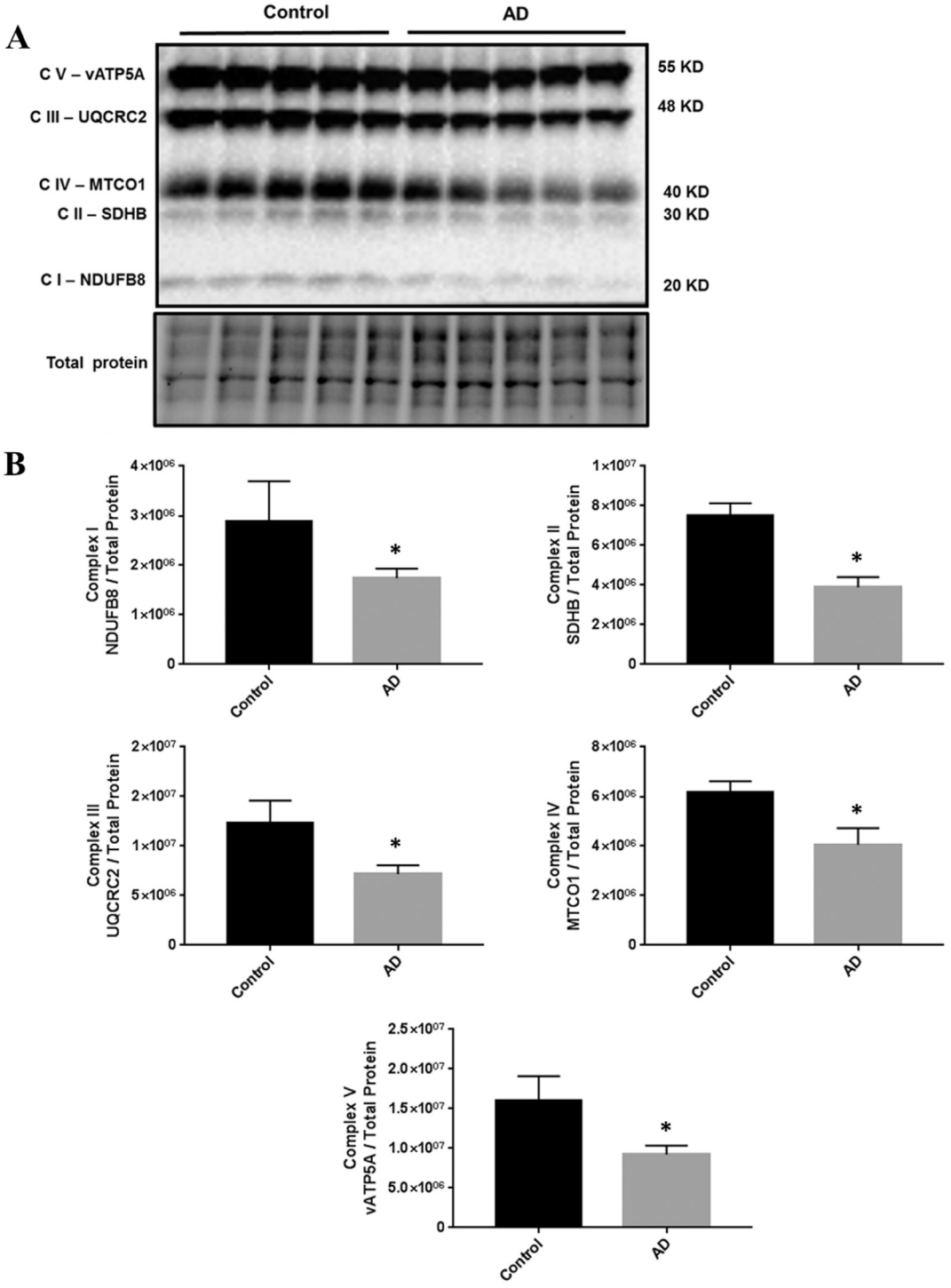

Fig. 3. Western blot results for OXPHOS proteins in isolated mitochondria from cortical piriform and insular of 11 months old AD and control mice. (A) Representative Western blot for NADH dehydrogenase beta subcomplex subunit 8 of Complex I (NDUFB8), succinate dehydrogenase subunit B of Complex II (SDHB), cytochrome *b*-c1 complex subunit 2 of Complex III (UQCRC2), Cytochrome c oxidase subunit 1 of Complex IV (MTCO1), and ATP synthase subunit alpha of Complex V (ATP5A). (B) Relative quantification for protein levels of Complex I-V in mitochondria from AD mice and their control groups normalized to total protein. Results are expressed as mean ± SD of n = 5 animals per group (*$p < .05$).

cortex (EC) (Fig. 5G), other central nervous system areas such as parasubiculum (PAS), sagulum (SAG) (Fig. 5H) as well as hippocampus (Fig. 5I). Negative control sections were obtained by omission of the primary antibody (Fig. 5F).

Immunohistochemistry staining did not detect astrocyte cells in the cortical insular and piriform of 3xTg mice or control (Fig. 6A, B). However, positive astrocyte staining was detected in the hippocampus and entorhinal cortex of both 3xTg and control mice (Fig. 6C-F). Immunoreactivity for microglia was detected in the cortical insular and piriform of control or 3xTg mice (Fig. 7). Furthermore, the volume density of GFAP immunoreactive astrocytes and Iba-1 immunoreactive microglia was increased in 3xTg mice compared to control mice.

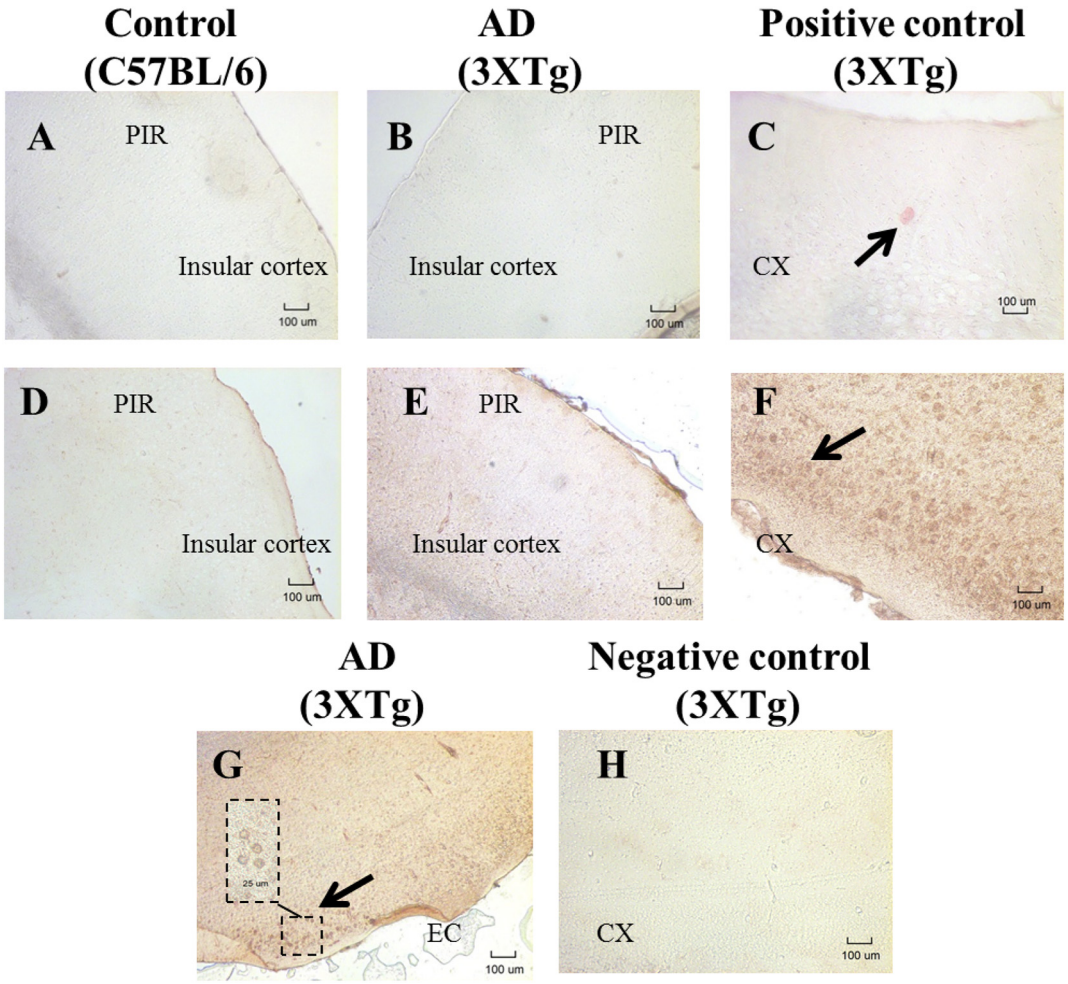

Fig. 4. Visualization of Aβ pathology in (10 μm) horizontal cryosections taken from the 11-month-old male AD mice (n = 5) and age-matched controls (n = 5) male mice. Congo red (CR) staining was utilized to detect extracellular Aβ deposits and immunohistochemical (IHC) staining was utilized to detect intracellular Aβ deposits. Panel A and B show the absence of extracellular amyloid plaques in the cortical insular cortex or cortical piriform (PIR) of either AD or control mice (A, B). Panel C shows a section from cortex of 14-month-old AD mice indicating the presence of Aβ plaques (positive control). No intracellular Aβ deposits were found in the cortical insular cortex or PIR of either AD or control mice (D, E). Panel F shows neurons immunoreactive for Aβ in the cortex (CX) of a 14-month-old AD mouse (positive control). Panel G shows positive intracellular Aβ deposits in the entorhinal cortex (EC) of AD mice. Negative control section from cortex of an 11-month-old AD mice indicating a lack of immunoreactivity with the primary antibody omitted (H). Images were captured at 10× magnification; scale bar distance shows 100 μm. Images magnified 100×, with boxed insert (B) magnified 400×. (For interpretation of the references to colour in this figure legend, the reader is referred to the web version of this article.)

4. Discussion

The current study showed no significant difference in *global* brain metabolic activity between AD and control groups; however, cortical *piriform* and *insular* regions of the brain in AD exhibited *significant* declines in FDG uptake (hypometabolism) as compared to that of the control group. In conjunction with hypometabolism in AD mice, the activity of terminal mitochondrial enzyme COX (complex IV) and protein expression of mitochondrial subunits (complex I-V) were significantly decreased in AD, which would be expected to compromise the site of oxidative phosphorylation and mitochondrial efficiency through the action of ATP synthesis.

Interestingly, we found significant decreases in complex I-V expression within regions of glucose hypometabolism. These findings suggest a relationship between ETC deficits and glucose hypometabolism. However, no amyloid plaques or neurofibrillary tangles (Thr 231, Ser 202/Thr 205) were found in regions in that exhibited hypometabolism (cortical piriform and insular regions). Moreover, Aβ deposits were found in the entorhinal cortex of 3xTg mice and neurofibrillary tangles were found in the entorhinal cortex, parasubiculum, sagulum, and hippocampus regions in 3xTg mice. Additionally, microglial cells, but not astrocytes were found in regions that exhibited hypometabolism. This finding provides evidence that there is an association between microglial pathology and hypometabolic activity, which suggested that brain inflammation occurs in AD sensitive brain regions.

The incidence of ETC deficiency and metabolic impairments before plaque and tangle formation indicates that bioenergetic impairments in cortical piriform and insular is an important early factor in the development of AD-like pathology (Aβ, tau, and astrocytes). These data also suggest that multiple aspects of bioenergetic impairments occur in a *region-dependent* manner.

Furthermore, deregulation of energy metabolism was demonstrated by measuring the activity of key enzymes involved in glycolytic pathway such as GAPDH, TCA cycle (CS), as well as oxidative phosphorylation (COX) in AD and control groups. A study by Lin et al., suggested that GAPDH dysregulation is a potential risk factor in AD onset (Lin et al., 2006). Several studies suggest a direct relationship between GAPDH and neurodegenerative disease-associated proteins, including amyloid plaques (Butterfield et al., 2010; Oyama et al., 2000; Schulze et al., 1993; Verdier et al., 2005). However, the relationship

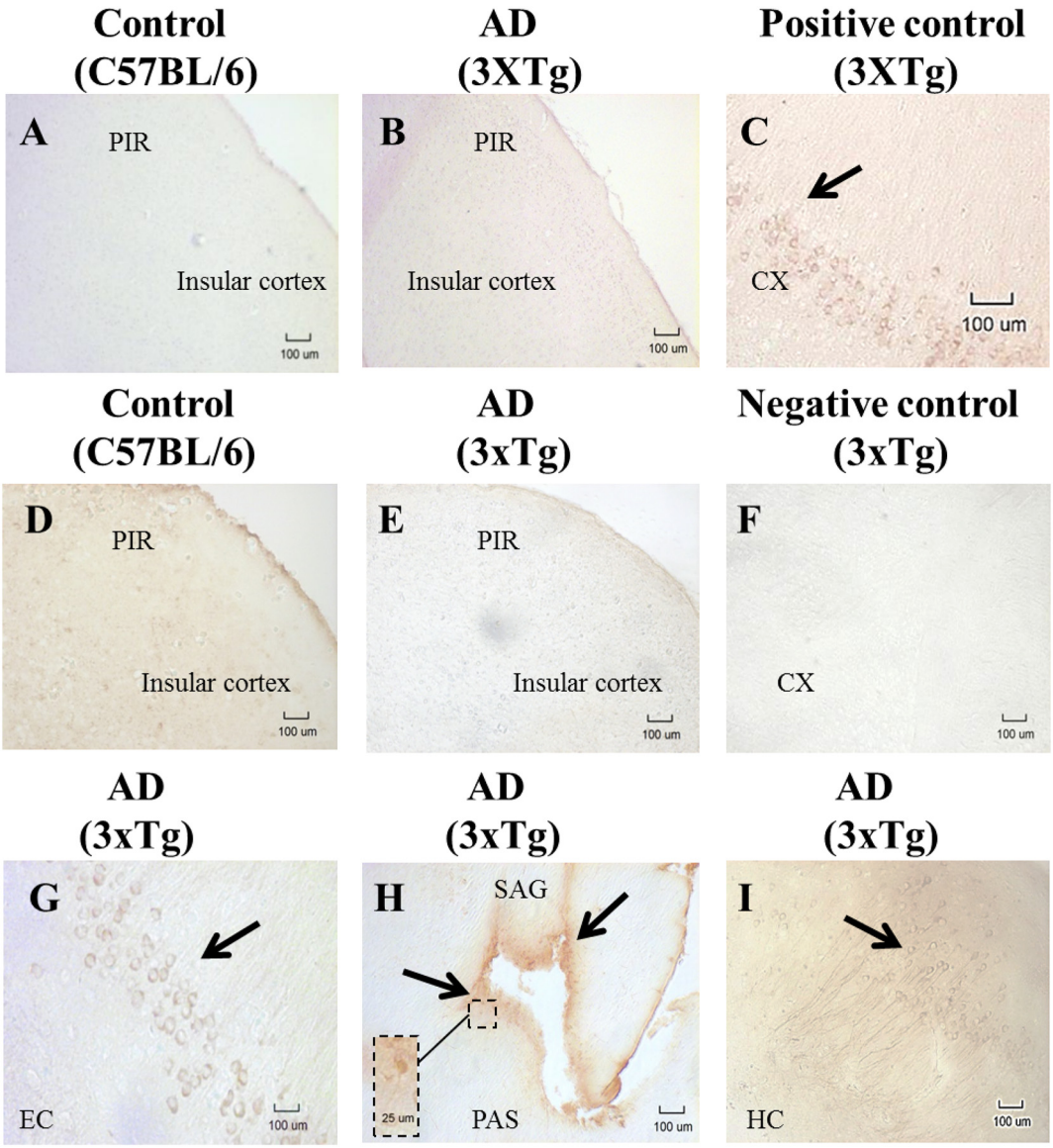

Fig. 5. Visualization of phospho-tau pathology (Thr 231) and (Ser202/Thr205) in (10 μm) horizontal cryosections taken from the 11-month-old male AD mice (n = 5) and age-matched controls (n = 5) male mice. Panel A and B present the absence of phospho-tau (Thr 231) in the cortical insular cortex or cortical piriform (PIR) of either AD or control mice. Panel D and E show the absence of phospho-tau (Ser202/Thr205) in the cortical insular cortex or cortical piriform (PIR) of either AD or control mice. Panel C shows a section from cortex of 14-month-old AD mice indicating the presence of tau tangles (positive control). Hyperphosphorylated tau was detected in the entorhinal cortex (EC), parasubiculum (PAS), sagulum (SAG), and hippocampus (HC) of AD mice (G-I). Negative control section from cortex of an 11-month-old AD mice indicating a lack of immunoreactivity with the primary antibody omitted (F). Images magnified 100×, with boxed insert (B) magnified 400×.

between GAPDH and Aβ in AD is not completely understood. A study by Naletova et al., suggested that only oxidized and denatured forms of GAPDH are able to accumulate in Aβ plaques and form highly stable complexes with amyloid plaques, demonstrating the direct involvement of GAPDH in plaque accumulation (Naletova et al., 2008). One study by Cumming and Schubert revealed that oxidative stress induced by amyloid plaques promotes oxidized and denatured forms of GAPDH binding and ultimately causes cell death (Cumming and Schubert, 2005). Our current enzymatic results showed no significant difference in the activity of GAPDH between AD and controls. Also, our histopathological examination showed an absence of Aβ plaques in AD and control samples. These data are in line with previous studies showing an association between dysregulation in GAPDH in areas with Aβ pathology. No correlational analysis was conducted between GAPDH and Aβ in this study due to an absence of Aβ plaques, as probed with congo red staining.

Consistent with a human study by Delbarba et al., the current study showed no significant differences in enzyme activity of CS in the AD compared to control groups. One other clinical study by Bubber et al., indicated that activities of some enzymes involved in the TCA cycle (e.g., CS, pyruvate dehydrogenase complex (PDHC), aconitase, isocitrate dehydrogenase (ICDH), and fumerase) were unchanged in schizophrenia patients as compared to that of the control groups (Bubber et al., 2011). These studies suggested that there is no significant correlation between enzymes of the TCA cycle and cognitive function. Furthermore, it has been shown that impaired function of the mitochondrial ETC as well as declined activity of COX (complex IV) may contribute to enhance oxidative damage and cell death in senescent tissues associated with aging (C. Zhang and Wong-Riley, 2000). In the current study, it was revealed that a significant reduction of COX activity in AD brain occurred (Mutisya et al., 1994). Decreased function of COX in ETC could contribute to the associated decrease in mitochondrial respiration, which is coupled with disrupted energy metabolism.

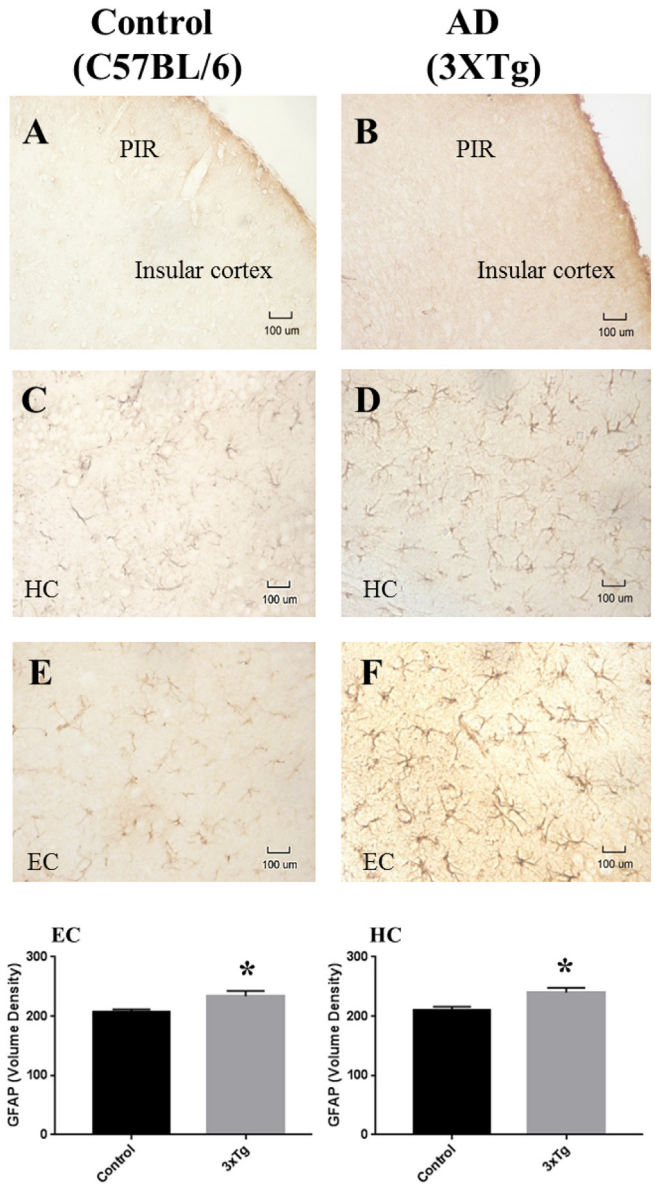

Fig. 6. Visualization of astrocytes in (10 μm) horizontal cryosections taken from the 11-month-old male AD mice (n = 5) and age-matched controls (n = 5) male mice. Panel A and B show the absence of astrocytes in the cortical insular cortex or cortical piriform (PIR) of either AD or control mice. Astrocyte cells were detected in the hippocampus (HC) and entorhinal cortex (EC) of both C57 and AD mice (C–F). GFAP immunoreactivity volume density values were quantified in the HC and EC regions of 3xTg compared to controls. Images were captured at 100× magnification; scale bar distance shows 100 μm.

A human study by Chandrasekaran et al., also suggested that a decrease in the expression of mitochondrial OXPHOS protein subunits causes down-regulation of oxidative phosphorylation machinery as well as decreased neuronal function in AD brains (Chandrasekaran et al., 1997). In alignment with Chandrasekaran's study, our Western blot analysis show down-regulation of mitochondrial subunits (complex I, II, III, IV, and V) in AD compared with their controls, suggesting a major role of oxidative phosphorylation in AD pathogenesis. These findings are also consistent with microarray analyses of aging in human AD and rodent AD models, demonstrating that proteins involved in mitochondrial oxidative phosphorylation are altered early in AD (Blalock et al., 2004; Liang et al., 2008; Reiman et al., 2004).

Previous studies revealed deficit in glucose uptakes is a critical factor of AD. It has been shown that hypometabolism is the major functional change found consistently in aged PDAPP, PSAPP, 3xTg, and 5xTg mouse models of AD (Macdonald et al., 2014; Nicholson et al., 2010; Reiman et al., 2000; Valla et al., 2006). Interestingly, hypermtabolism also has been found in relatively younger transgenic mice models such as APP(Tg2576), APP (Tg2576)xPS1M146L, B6.PS2APP, 3xTg mice, and 5XFAD (Brendel et al., 2016; Cristea et al., 2013; Luo et al., 2012; Macdonald et al., 2014; Poisnel et al., 2012; Rojas et al., 2013; Sancheti et al., 2014; Valla et al., 2006). Hypermetabolism is correlated with neuroinflammation which is in association with the amyloidosis in this transgenic AD mouse model (Brendel et al., 2016). Inconsistent metabolic activities are depending on the age, disease progression and type of AD mouse model. Additionally, there are no consistent regional metabolic patterns found across various studies. The inconsistencies between studies may be due to differences in laboratory colony of origin, sample size, age and sex of subjects, image analysis procedures, as well as differences in AD-like brain pathology across mouse models. For example, the 3xTg model, used in the present study, is the only mouse model to recapitulate the neurofibrillary pathology that is a hallmark of AD. Interestingly, our current findings of hypometabolism in the 3xTg model are also closely in line with human FDG-PET studies (Desgranges et al., 2007; Joffe et al., 2012). These findings suggest that human PET imaging is capable of detecting early aberration in glucose metabolism in AD and that hypometabolism can be an early biomarker for AD diagnosis. Current metabolic analysis also shows severe hypometabolism in the cortical piriform and insular of 3xTg mice relative to controls. The insular cortex is highly interconnected with different parts of the brain and is involved in perceptual processing, including somatosensory, viscerosensory, interoceptive, visceromotor, and olfactory processing as well as cognitive function (Augustine, 1996; Bonthius et al., 2005; Critchley, 2005; Kurth et al., 2010; Showers and Lauer, 1961). Interestingly, all aforementioned neurologic functions and processing can be impaired in individuals with AD. Several neuroimaging and neuropathological studies in AD show a specific and early impairment in olfaction that is mediated by the piriform cortex (Kareken et al., 2001; Li et al., 2010; Wang et al., 2010). Moreover, pathological and neuroimaging studies have suggested that piriform cortex dysfunction is responsible for the noted olfactory impairments in AD, and that this is related to memory impairment in AD (Augustine, 1996; Burns, 2000; Devanand et al., 2000; Li et al., 2010; Suzuki et al., 2004).

In mammals, cortical piriform and insular regions have shared connections with the olfactory cortex, which is substantially impaired in AD patients (Carmichael et al., 1994; Christen-Zaech et al., 2003; Mesholam et al., 1998; Michelini and Flynn, 1999; Peters et al., 2003; Zatorre et al., 1992). Interestingly, olfaction is unique in the process of neurogenesis and neurodegenerative diseases often have olfactory loss early on in the course of their disorder (Gallarda and Lledo, 2012). Such critical properties of olfaction and neurogenesis may underlie improved learning and memory functions observed in diseases with cognitive impairments such as AD. Therefore, it is suggested that early functional deficits in the cortical piriform and insular regions should be considered as an appropriate biomarker in the testing of novel interventions.

Interestingly, neuropathological studies have shown that amyloid and tangle pathology develop in a gender-dependent fashion [10–12]. For example, earlier pathological studies noted amyloid plaque deposits in 11-month-old female, but not male, 3xTg mice (Mastrangelo and Bowers, 2008; Nicholson et al., 2010; Oh et al., 2010). A report by Nicholson et al., noted that only 40% of 3xTg mice (12-months old) in their study had evidence of plaque formation (Nicholson et al., 2010). Discrepancy in results may be due to mixing of both male and female subjects, as sex-specific data was not provided. In light of these results, we chose to evaluate brain metabolism in relation to AD pathology in male 3xTg mice only.

Several studies have shown that Aβ protein accumulates in both extracellular and intracellular spaces, ultimately leading to plaque formation (LaFerla et al., 1995; Skovronsky et al., 1998). Current

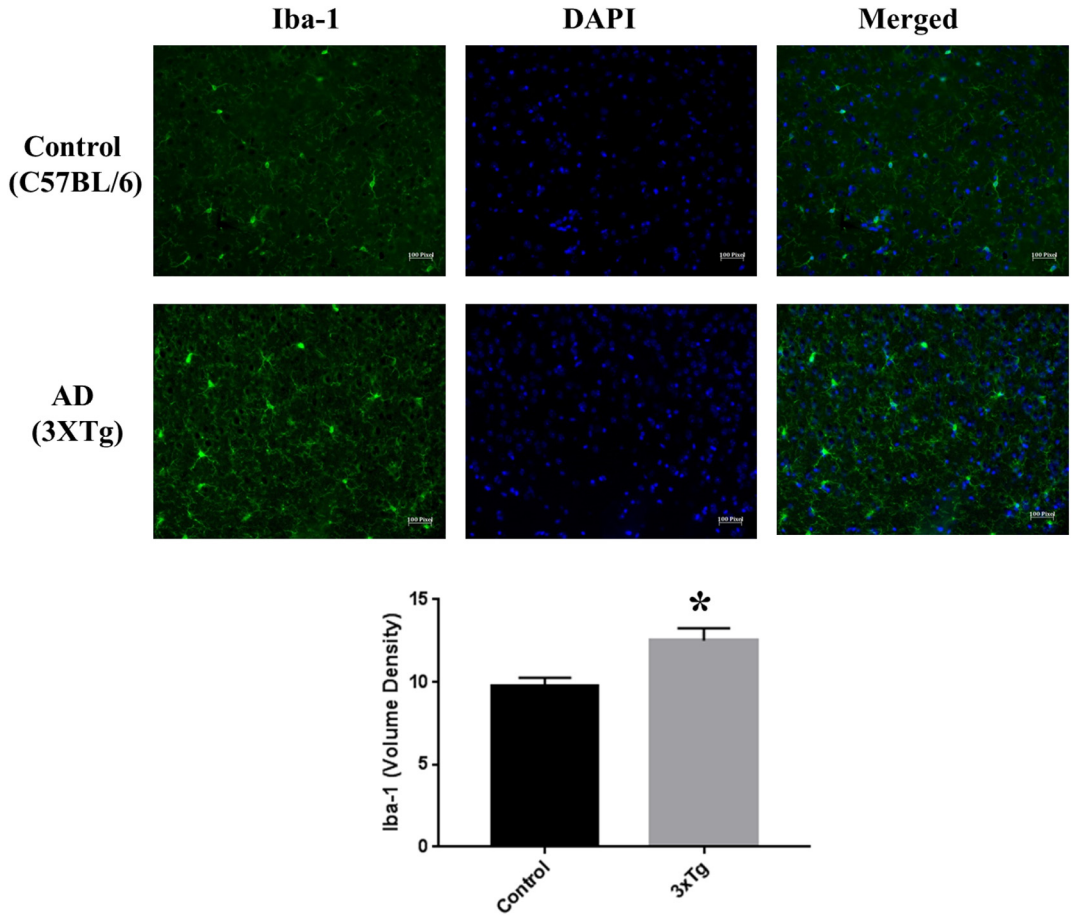

Fig. 7. Immunofluorescence images depicting Iba1-labeled microglia cells (green) in the cortical insular cortex or cortical piriform of 11-month-old male AD mice (n = 5) and age-matched controls (n = 5) male mice (nuclei were labeled blue with DAPI). The volume density of Iba-1 immunofluorescence was quantified in the hypometabolic region of 3xTg compared to controls. Results are expressed as mean ± SD of n = 5 animals per group (*$p < .05$). Scale bar = 100 pixel. (For interpretation of the references to colour in this figure legend, the reader is referred to the web version of this article.)

findings show no extracellular plaques in 3xTg and control groups, but intracellular Aβ deposits were detected in the entorhinal cortex of 3xTg. Initial characterization studies of AD state that Aβ peptides are first formed intracellularly, than as 3xTg mice age, they exhibit extracellular plaque load (Cummings et al., 1992; Oddo et al., 2006). However, there has been considerable debate regarding the Aβ accumulations in AD. Further characterizations of AD progression in 3xTg revealed that Aβ pathology appears first in the cortex and then progress to the hippocampus (Oddo et al., 2003a). This evidence is in line with the results of our pathological experiments. Similarly, 3xTg mice in the current study exhibited intracellular Aβ deposits in the entorhinal cortex at 11 months old.

Additionally, immunohistochemistry of tau was carried out to detect tau tangles in AD mouse brains. Our results of tau pathology in AD mice are consistent with previous human and mouse studies (de Calignon et al., 2012; Harris et al., 2012; Hohsfield et al., 2014; Irmler et al., 2012; Kida et al., 1992; Liu et al., 2012; Wu et al., 2015). A recent study reported histopathology in 3xTg mice used a common antibody, AT8, to evaluate the extent of neurofibrillary tangle pathology in paraformaldehyde fixed brains (Nicholson et al., 2010). However, they reported a marked decreased in immunoreactivity with AT8 in 3xTg mice, whereas immunohistochemistry with AT180 revealed intense and widespread staining of neurons (Nicholson et al., 2010; Petry et al., 2014). Different commercially available tau antibodies (i.e. AT8, AT180) show different immunoreactivity for hyperphosphorylated tau protein (Petry et al., 2014). Likely, AT8 phospho-epitope is more sensitive to phosphatase activity than AT180 phosphorylation sites, resulting in less staining in tangle-containing 3xTg neurons (Garver et al., 1994). Utilizing AT180 in the present study revealed an intense and widespread staining of neurons in 3xTg brain sections. Thus, methodological considerations may affect the interpretation of the relationship between AD-related neuropathology and brain metabolism, as measured by PET imaging.

Overall, our findings revealed no association between pathology and metabolic changes in male 3xTg mice. The most likely explanation for a lack of association between both measures is dysregulation of glucose metabolism associated with the development of AD that is present earlier than AD pathology. Since there are prominent gender-differences in the prevalence of AD, further studies are required to investigate metabolic and histological alterations in AD utilizing female 3xTg mice.

5. Conclusions

The major finding of this study is the region-specific brain hypometabolism in aged 3xTg mice (11 months old) as compared with age-matched control mice. These results are in contrast to brain hypermetabolism in the relatively younger 3xTg mice (7 months old) (Sancheti et al., 2014). Inconsistent metabolic activities are depending on the age or disease progression. It is suggested that 3xTg mice have been shown to transition from a state of hypermetabolism, during the early stages of amyloid plaque deposition, to a hypometabolism state, following significant amyloid deposition. Additionally, it is suggested that hypometabolism transition may be occurring as a compensatory mechanism

in response to the damage of neurons, before high amyloid deposition takes place in aged 3xTg. Furthermore, this study suggests that regional brain hypometabolism is unrelated to amyloid plaque, tau tangle deposition as well as astrocyte pathology. However, there is an association between neuroinflammatory pathological markers (microglial) and hypometabolism in the early stage of AD.

Additionally, there is an association between glucose hypometabolism and reduced mitochondrial complex I-V functioning, but no association between metabolic activity and histopathology of Aβ, tau and astrocyte at early time points. This lack of association suggests that alterations in brain energy metabolism occur prior to AD pathology in sensitive brain regions. These results also suggest that hypometabolism in cortical piriform and insular regions functions as a useful biomarker that could facilitate testing of novel interventions early in disease progression.

Conflict of interest statement

The authors declare that the research was conducted in the absence of any commercial or financial relationships that could be construed as a potential conflict of interest.

Author contributions

AA designed the experiments and wrote the manuscript. AA was involved in statistical analysis and interpretation of the data. AA isolated mitochondria, conducted Western blot experiments, cyrosectioning, congo staining, immunohistochemistry, immunofluorescence and enzyme assays (COX, GAPDH, CS). GS and ALG were involved in carrying out the FDG-PET imaging. JHK analyzed PET data and created PET image. AA and WS were involved in immunohistochemistry and microscopy. JD and CP were involved in dissections. BCA was involved in conception, study design as well as manuscript revision.

Acknowledgments

This work was supported by a Research Manitoba Fellowship (to Dr. Adlimoghaddam), the St. Boniface Hospital Research Foundation (Grant Nos.1406-3216 and 1410-3216), the Alzheimer's Society of Manitoba, Research Manitoba, and The Honourable Douglas and Patricia Everett and Royal Canadian Properties Limited Endowment Fund (Grant No. 1403-3131). Dr. Albensi holds the Honourable Douglas and Patricia Everett and Royal Canadian Properties Limited Endowment Fund Chair and the Manitoba Dementia Research Chair (funded by the Alzheimer's Soc. of Manitoba & Research Manitoba) and is a Research Affiliate of the Centre on Aging at the University of Manitoba. We thank Dr. Darrell Smith for his kind support in preparation of the animal protocol.

References

Arriagada, P.V., Marzloff, K., Hyman, B.T., 1992. Distribution of Alzheimer-type pathologic changes in nondemented elderly individuals matches the pattern in Alzheimer's disease. Neurology 42 (9), 1681–1688.

Ashburner, J., Friston, K.J., 2000. Voxel-based morphometry—the methods. Neuroimage 11 (6 Pt 1), 805–821. https://doi.org/10.1006/nimg.2000.0582.

Ashburner, J., Friston, K.J., 2005. Unified segmentation. Neuroimage 26 (3), 839–851. https://doi.org/10.1016/j.neuroimage.2005.02.018.

Ashe, K.H., Zahs, K.R., 2010. Probing the biology of Alzheimer's disease in mice. Neuron 66 (5), 631–645. https://doi.org/10.1016/j.neuron.2010.04.031.

Ashraf, A., Fan, Z., Brooks, D.J., Edison, P., 2015. Cortical hypermetabolism in MCI subjects: a compensatory mechanism? Eur. J. Nucl. Med. Mol. Imaging 42 (3), 447–458. https://doi.org/10.1007/s00259-014-2919-z.

Augustine, J.R., 1996. Circuitry and functional aspects of the insular lobe in primates including humans. Brain Res. Brain Res. Rev. 22 (3), 229–244.

Backes, H., Walberer, M., Ladwig, A., Rueger, M.A., Neumaier, B., Endepols, H., ... Graf, R., 2016. Glucose consumption of inflammatory cells masks metabolic deficits in the brain. Neuroimage 128, 54–62. https://doi.org/10.1016/j.neuroimage.2015.12.044.

Baek, H., Ye, M., Kang, G. H., Lee, C., Lee, G., Choi, D. B., … Bae, H. (2016). Neuroprotective effects of CD4 + CD25 + Foxp3 + regulatory T cells in a 3xTg-AD Alzheimer's disease model. *Oncotarget, 7*(43), 69347-69357. Doi: 10.18632/oncotarget.12469.

Ballatore, C., Lee, V.M., Trojanowski, J.Q., 2007. Tau-mediated neurodegeneration in Alzheimer's disease and related disorders. Nat. Rev. Neurosci. 8 (9), 663–672. https://doi.org/10.1038/nrn2194.

Beach, T.G., Monsell, S.E., Phillips, L.E., Kukull, W., 2012. Accuracy of the clinical diagnosis of Alzheimer disease at National Institute on Aging Alzheimer Disease Centers, 2005–2010. J. Neuropathol. Exp. Neurol. 71 (4), 266–273. https://doi.org/10.1097/NEN.0b013e31824b211b.

Blalock, E.M., Geddes, J.W., Chen, K.C., Porter, N.M., Markesbery, W.R., Landfield, P.W., 2004. Incipient Alzheimer's disease: microarray correlation analyses reveal major transcriptional and tumor suppressor responses. Proc. Natl. Acad. Sci. U. S. A. 101 (7), 2173–2178. https://doi.org/10.1073/pnas.0308512100.

Blass, J.P., Sheu, R.K., Gibson, G.E., 2000. Inherent abnormalities in energy metabolism in Alzheimer disease. Interaction with cerebrovascular compromise. Ann. N. Y. Acad. Sci. 903, 204–221.

Bohnen, N.I., Jahn, K., 2013. Imaging: what can it tell us about parkinsonian gait? Mov. Disord. 28 (11), 1492–1500. https://doi.org/10.1002/mds.25534.

Bonthius, D.J., Solodkin, A., Van Hoesen, G.W., 2005. Pathology of the insular cortex in Alzheimer disease depends on cortical architecture. J. Neuropathol. Exp. Neurol. 64 (10), 910–922.

Braak, H., Braak, E., 1991. Neuropathological stageing of Alzheimer-related changes. Acta Neuropathol. 82 (4), 239–259.

Braak, H., Braak, E., 1996. Development of Alzheimer-related neurofibrillary changes in the neocortex inversely recapitulates cortical myelogenesis. Acta Neuropathol. 92 (2), 197–201.

Brendel, M., Probst, F., Jaworska, A., Overhoff, F., Korzhova, V., Albert, N.L., ... Rominger, A., 2016. Glial activation and glucose metabolism in a transgenic amyloid mouse model: a triple-tracer PET study. J. Nucl. Med. 57 (6), 954–960. https://doi.org/10.2967/jnumed.115.167858.

Brown, R.K., Bohnen, N.I., Wong, K.K., Minoshima, S., Frey, K.A., 2014. Brain PET in suspected dementia: patterns of altered FDG metabolism. Radiographics 34 (3), 684–701. https://doi.org/10.1148/rg.343135065.

Bubber, P., Haroutunian, V., Fisch, G., Blass, J.P., Gibson, G.E., 2005. Mitochondrial abnormalities in Alzheimer brain: mechanistic implications. Ann. Neurol. 57 (5), 695–703. https://doi.org/10.1002/ana.20474.

Bubber, P., Hartounian, V., Gibson, G.E., Blass, J.P., 2011. Abnormalities in the tricarboxylic acid (TCA) cycle in the brains of schizophrenia patients. Eur. Neuropsychopharmacol. 21 (3), 254–260. https://doi.org/10.1016/j.euroneuro.2010.10.007.

Burns, A., 2000. Might olfactory dysfunction be a marker of early Alzheimer's disease? Lancet 355 (9198), 84–85. https://doi.org/10.1016/S0140-6736(99)90402-6.

Busche, M.A., Chen, X., Henning, H.A., Reichwald, J., Staufenbiel, M., Sakmann, B., Konnerth, A., 2012. Critical role of soluble amyloid-beta for early hippocampal hyperactivity in a mouse model of Alzheimer's disease. Proc. Natl. Acad. Sci. U. S. A. 109 (22), 8740–8745. https://doi.org/10.1073/pnas.1206171109.

Butterfield, D.A., Hardas, S.S., Lange, M.L., 2010. Oxidatively modified glyceraldehyde-3-phosphate dehydrogenase (GAPDH) and Alzheimer's disease: many pathways to neurodegeneration. J. Alzheimers Dis. 20 (2), 369–393. https://doi.org/10.3233/JAD-2010-1375.

Calsolaro, V., Edison, P., 2016. Neuroinflammation in Alzheimer's disease: current evidence and future directions. Alzheimers Dement. 12 (6), 719–732. https://doi.org/10.1016/j.jalz.2016.02.010.

Carmichael, S.T., Clugnet, M.C., Price, J.L., 1994. Central olfactory connections in the macaque monkey. J. Comp. Neurol. 346 (3), 403–434. https://doi.org/10.1002/cne.903460306.

Catafau, A.M., Bullich, S., 2015. Amyloid PET imaging: applications beyond Alzheimer's disease. Clin. Transl. Imaging 3 (1), 39–55. https://doi.org/10.1007/s40336-014-0098-3.

Chandrasekaran, K., Hatanpaa, K., Rapoport, S.I., Brady, D.R., 1997. Decreased expression of nuclear and mitochondrial DNA-encoded genes of oxidative phosphorylation in association neocortex in Alzheimer disease. Brain Res. Mol. Brain Res. 44 (1), 99–104.

Chetelat, G., Desgranges, B., Landeau, B., Mezenge, F., Poline, J.B., de la Sayette, V., ... Baron, J.C., 2008. Direct voxel-based comparison between grey matter hypometabolism and atrophy in Alzheimer's disease. Brain 131 (Pt 1), 60–71. https://doi.org/10.1093/brain/awm288.

Christen-Zaech, S., Kraftsik, R., Pillevuit, O., Kiraly, M., Martins, R., Khalili, K., Miklossy, J., 2003. Early olfactory involvement in Alzheimer's disease. Can. J. Neurol. Sci. 30 (1), 20–25.

Cristea, S., Freyvert, Y., Santiago, Y., Holmes, M.C., Urnov, F.D., Gregory, P.D., Cost, G.J., 2013. In vivo cleavage of transgene donors promotes nuclease-mediated targeted integration. Biotechnol. Bioeng. 110 (3), 871–880. https://doi.org/10.1002/bit.24733.

Critchley, H.D., 2005. Neural mechanisms of autonomic, affective, and cognitive integration. J. Comp. Neurol. 493 (1), 154–166. https://doi.org/10.1002/cne.20749.

Cumming, R.C., Schubert, D., 2005. Amyloid-beta induces disulfide bonding and aggregation of GAPDH in Alzheimer's disease. FASEB J. 19 (14), 2060–2062. https://doi.org/10.1096/fj.05-4195fje.

Cummings, B.J., Su, J.H., Geddes, J.W., Van Nostrand, W.E., Wagner, S.L., Cunningham, D.D., Cotman, C.W., 1992. Aggregation of the amyloid precursor protein within degenerating neurons and dystrophic neurites in Alzheimer's disease. Neuroscience 48 (4), 763–777.

de Calignon, A., Polydoro, M., Suarez-Calvet, M., William, C., Adamowicz, D.H., Kopeikina, K.J., ... Hyman, B.T., 2012. Propagation of tau pathology in a model of

early Alzheimer's disease. Neuron 73 (4), 685–697. https://doi.org/10.1016/j.neuron.2011.11.033.
De Santi, S., de Leon, M.J., Rusinek, H., Convit, A., Tarshish, C.Y., Roche, A., ... Fowler, J., 2001. Hippocampal formation glucose metabolism and volume losses in MCI and AD. Neurobiol. Aging 22 (4), 529–539.
Del Sole, A., Clerici, F., Chiti, A., Lecchi, M., Mariani, C., Maggiore, L., ... Lucignani, G., 2008. Individual cerebral metabolic deficits in Alzheimer's disease and amnestic mild cognitive impairment: an FDG PET study. Eur. J. Nucl. Med. Mol. Imaging 35 (7), 1357–1366. https://doi.org/10.1007/s00259-008-0773-6.
Delacourte, A., David, J.P., Sergeant, N., Buee, L., Wattez, A., Vermersch, P., ... Di Menza, C., 1999. The biochemical pathway of neurofibrillary degeneration in aging and Alzheimer's disease. Neurology 52 (6), 1158–1165.
Desgranges, B., Matuszewski, V., Piolino, P., Chetelat, G., Mezenge, F., Landeau, B., ... Eustache, F., 2007. Anatomical and functional alterations in semantic dementia: a voxel-based MRI and PET study. Neurobiol. Aging 28 (12), 1904–1913. https://doi.org/10.1016/j.neurobiolaging.2006.08.006.
Devanand, D.P., Michaels-Marston, K.S., Liu, X., Pelton, G.H., Padilla, M., Marder, K., ... Mayeux, R., 2000. Olfactory deficits in patients with mild cognitive impairment predict Alzheimer's disease at follow-up. Am. J. Psychiatry 157 (9), 1399–1405. https://doi.org/10.1176/appi.ajp.157.9.1399.
Duara, R., Grady, C., Haxby, J., Sundaram, M., Cutler, N.R., Heston, L., ... Rapoport, S.I., 1986. Positron emission tomography in Alzheimer's disease. Neurology 36 (7), 879–887.
Eikelenboom, P., Bate, C., Van Gool, W.A., Hoozemans, J.J., Rozemuller, J.M., Veerhuis, R., Williams, A., 2002. Neuroinflammation in Alzheimer's disease and prion disease. Glia 40 (2), 232–239. https://doi.org/10.1002/glia.10146.
El Kadmiri, N., Slassi, I., El Moutawakil, B., Nadifi, S., Tadevosyan, A., Hachem, A., Soukri, A., 2014. Glyceraldehyde-3-phosphate dehydrogenase (GAPDH) and Alzheimer's disease. Pathol. Biol. (Paris) 62 (6), 333–336. https://doi.org/10.1016/j.patbio.2014.08.002.
Ellis, R.J., Olichney, J.M., Thal, L.J., Mirra, S.S., Morris, J.C., Beekly, D., Heyman, A., 1996. Cerebral amyloid angiopathy in the brains of patients with Alzheimer's disease: the CERAD experience, part XV. Neurology 46 (6), 1592–1596.
Foster, N.L., Chase, T.N., Mansi, L., Brooks, R., Fedio, P., Patronas, N.J., Di Chiro, G., 1984. Cortical abnormalities in Alzheimer's disease. Ann. Neurol. 16 (6), 649–654. https://doi.org/10.1002/ana.410160605.
Friedland, R.P., Budinger, T.F., Ganz, E., Yano, Y., Mathis, C.A., Koss, B., ... Derenzo, S.E., 1983. Regional cerebral metabolic alterations in dementia of the Alzheimer type: positron emission tomography with [18F]fluorodeoxyglucose. J. Comput. Assist. Tomogr. 7 (4), 590–598.
Gallarda, B.W., Lledo, P.M., 2012. Adult neurogenesis in the olfactory system and neurodegenerative disease. Curr. Mol. Med. 12 (10), 1253–1260.
Garver, T.D., Harris, K.A., Lehman, R.A., Lee, V.M., Trojanowski, J.Q., Billingsley, M.L., 1994. Tau phosphorylation in human, primate, and rat brain: evidence that a pool of tau is highly phosphorylated in vivo and is rapidly dephosphorylated in vitro. J. Neurochem. 63 (6), 2279–2287.
Gibson, G.E., Park, L.C., Sheu, K.F., Blass, J.P., Calingasan, N.Y., 2000. The alpha-ketoglutarate dehydrogenase complex in neurodegeneration. Neurochem. Int. 36 (2), 97–112.
Glabe, C.C., 2005. Amyloid accumulation and pathogensis of Alzheimer's disease: significance of monomeric, oligomeric and fibrillar Abeta. Subcell Biochem. 38, 167–177.
Goertzen, A., Stortz, G., Thiessen, J., Bishop, D., Khan, M.S., Kozlowski, P., ... Thompson, C., 2015. First results from a high-resolution small animal PET insert for PET/MRI imaging. EJNMMI Phys. 2 (Suppl. 1), A54. https://doi.org/10.1186/2197-7364-2-S1-A54.
Hansson, O., Gouras, G., 2016. Brain activity and Alzheimer's disease: a complex relationship. Brain 139 (Pt 8), 2109–2110. https://doi.org/10.1093/brain/aww146.
Hardy, J., Selkoe, D.J., 2002. The amyloid hypothesis of Alzheimer's disease: progress and problems on the road to therapeutics. Science 297 (5580), 353–356. https://doi.org/10.1126/science.1072994.
Harris, J.A., Koyama, A., Maeda, S., Ho, K., Devidze, N., Dubal, D.B., ... Mucke, L., 2012. Human P301L-mutant tau expression in mouse entorhinal-hippocampal network causes tau aggregation and presynaptic pathology but no cognitive deficits. PLoS One 7 (9), e45881. https://doi.org/10.1371/journal.pone.0045881.
Harry, G.J., Hooth, M.J., Vallant, M., Behl, M., Travlos, G.S., Howard, J.L., ... Mouton, P.R., 2014. Developmental neurotoxicity of 3,3′,4,4′-tetrachloroazobenzene with thyroxine deficit: sensitivity of glia and dentate granule neurons in the absence of behavioral changes. Toxics 2 (3), 496–532. https://doi.org/10.3390/toxics2030496.
Hatami, A., Albay 3rd, R., Monjazeb, S., Milton, S., Glabe, C., 2014. Monoclonal antibodies against Abeta42 fibrils distinguish multiple aggregation state polymorphisms in vitro and in Alzheimer disease brain. J. Biol. Chem. 289 (46), 32131–32143. https://doi.org/10.1074/jbc.M114.594846.
Haxby, J.V., Grady, C.L., Duara, R., Schlageter, N., Berg, G., Rapoport, S.I., 1986. Neocortical metabolic abnormalities precede nonmemory cognitive defects in early Alzheimer's-type dementia. Arch. Neurol. 43 (9), 882–885.
Heneka, M.T., Carson, M.J., El Khoury, J., Landreth, G.E., Brosseron, F., Feinstein, D.L., ... Kummer, M.P., 2015. Neuroinflammation in Alzheimer's disease. Lancet Neurol. 14 (4), 388–405. https://doi.org/10.1016/S1474-4422(15)70016-5.
Hernandez-Zimbron, L.F., Perez-Hernandez, M., Torres-Romero, A., Gorostieta-Salas, E., Gonzalez-Salinas, R., Gulias-Canizo, R., ... Zenteno, E., 2017. Markers of Alzheimer's disease in primary visual cortex in normal aging in mice. Biomed. Res. Int. 2017, 3706018. https://doi.org/10.1155/2017/3706018.
Hohsfield, L.A., Daschil, N., Oradd, G., Stromberg, I., Humpel, C., 2014. Vascular pathology of 20-month-old hypercholesterolemia mice in comparison to triple-transgenic and APPSwDI Alzheimer's disease mouse models. Mol. Cell. Neurosci. 63, 83–95. https://doi.org/10.1016/j.mcn.2014.10.006.
Irmler, M., Gentier, R.J., Dennissen, F.J., Schulz, H., Bolle, I., Holter, S.M., ... Beckers, J., 2012. Long-term proteasomal inhibition in transgenic mice by UBB(+1) expression results in dysfunction of central respiration control reminiscent of brainstem neuropathology in Alzheimer patients. Acta Neuropathol. 124 (2), 187–197. https://doi.org/10.1007/s00401-012-1003-7.
Ishii, K., Sasaki, M., Kitagaki, H., Yamaji, S., Sakamoto, S., Matsuda, K., Mori, E., 1997. Reduction of cerebellar glucose metabolism in advanced Alzheimer's disease. J. Nucl. Med. 38 (6), 925–928.
Jack Jr., C.R., Knopman, D.S., Jagust, W.J., Shaw, L.M., Aisen, P.S., Weiner, M.W., ... Trojanowski, J.Q., 2010. Hypothetical model of dynamic biomarkers of the Alzheimer's pathological cascade. Lancet Neurol. 9 (1), 119–128. https://doi.org/10.1016/S1474-4422(09)70299-6.
Jeong, Y.J., Yoon, H.J., Kang, D.Y., 2017. Assessment of change in glucose metabolism in white matter of amyloid-positive patients with Alzheimer disease using F-18 FDG PET. Medicine (Baltimore) 96 (48), e9042. https://doi.org/10.1097/MD.0000000000009042.
Joffe, H., Deckersbach, T., Lin, N.U., Makris, N., Skaar, T.C., Rauch, S.L., ... Hall, J.E., 2012. Metabolic activity in the insular cortex and hypothalamus predicts hot flashes: an FDG-PET study. J. Clin. Endocrinol. Metab. 97 (9), 3207–3215. https://doi.org/10.1210/jc.2012-1413.
Kareken, D.A., Doty, R.L., Moberg, P.J., Mosnik, D., Chen, S.H., Farlow, M.R., Hutchins, G.D., 2001. Olfactory-evoked regional cerebral blood flow in Alzheimer's disease. Neuropsychology 15 (1), 18–29.
Kida, E., Barcikowska, M., Niemczewska, M., 1992. Immunohistochemical study of a case with progressive supranuclear palsy without ophthalmoplegia. Acta Neuropathol. 83 (3), 328–332.
Kim, E.J., Cho, S.S., Jeong, Y., Park, K.C., Kang, S.J., Kang, E., ... Na, D.L., 2005. Glucose metabolism in early onset versus late onset Alzheimer's disease: an SPM analysis of 120 patients. Brain 128 (Pt 8), 1790–1801. https://doi.org/10.1093/brain/awh539.
Klupp, E., Grimmer, T., Tahmasian, M., Sorg, C., Yakushev, I., Yousefi, B.H., ... Forster, S., 2015. Prefrontal hypometabolism in Alzheimer disease is related to longitudinal amyloid accumulation in remote brain regions. J. Nucl. Med. 56 (3), 399–404. https://doi.org/10.2967/jnumed.114.149302.
Kurth, F., Zilles, K., Fox, P.T., Laird, A.R., Eickhoff, S.B., 2010. A link between the systems: functional differentiation and integration within the human insula revealed by meta-analysis. Brain Struct. Funct. 214 (5–6), 519–534. https://doi.org/10.1007/s00429-010-0255-z.
LaFerla, F.M., Tinkle, B.T., Bieberich, C.J., Haudenschild, C.C., Jay, G., 1995. The Alzheimer's A beta peptide induces neurodegeneration and apoptotic cell death in transgenic mice. Nat. Genet. 9 (1), 21–30. https://doi.org/10.1038/ng0195-21.
Li, W., Howard, J.D., Gottfried, J.A., 2010. Disruption of odour quality coding in piriform cortex mediates olfactory deficits in Alzheimer's disease. Brain 133 (9), 2714–2726. https://doi.org/10.1093/brain/awq209.
Liang, W.S., Reiman, E.M., Valla, J., Dunckley, T., Beach, T.G., Grover, A., ... Stephan, D.A., 2008. Alzheimer's disease is associated with reduced expression of energy metabolism genes in posterior cingulate neurons. Proc. Natl. Acad. Sci. U. S. A. 105 (11), 4441–4446. https://doi.org/10.1073/pnas.0709259105.
Lin, P.I., Martin, E.R., Bronson, P.G., Browning-Large, C., Small, G.W., Schmechel, D.E., ... Pericak-Vance, M.A., 2006. Exploring the association of glyceraldehyde-3-phosphate dehydrogenase gene and Alzheimer disease. Neurology 67 (1), 64–68. https://doi.org/10.1212/01.wnl.0000223438.90113.4e.
Liu, L., Drouet, V., Wu, J.W., Witter, M.P., Small, S.A., Clelland, C., Duff, K., 2012. Trans-synaptic spread of tau pathology in vivo. PLoS One 7 (2), e31302. https://doi.org/10.1371/journal.pone.0031302.
Luo, F., Rustay, N.R., Ebert, U., Hradil, V.P., Cole, T.B., Llano, D.A., ... Day, M., 2012. Characterization of 7- and 19-month-old Tg2576 mice using multimodal in vivo imaging: limitations as a translatable model of Alzheimer's disease. Neurobiol. Aging 33 (5), 933–944. https://doi.org/10.1016/j.neurobiolaging.2010.08.005.
Ma, Y., Hof, P.R., Grant, S.C., Blackband, S.J., Bennett, R., Slatest, L., ... Benveniste, H., 2005. A three-dimensional digital atlas database of the adult C57BL/6J mouse brain by magnetic resonance microscopy. Neuroscience 135 (4), 1203–1215. https://doi.org/10.1016/j.neuroscience.2005.07.014.
Macdonald, I.R., DeBay, D.R., Reid, G.A., O'Leary, T.P., Jollymore, C.T., Mawko, G., ... Darvesh, S., 2014. Early detection of cerebral glucose uptake changes in the 5XFAD mouse. Curr. Alzheimer Res. 11 (5), 450–460.
Marcus, C., Mena, E., Subramaniam, R.M., 2014. Brain PET in the diagnosis of Alzheimer's disease. Clin. Nucl. Med. *39* (10), e413–e422. quiz e423-416. https://doi.org/10.1097/RLU.0000000000000547.
Mastrangelo, M.A., Bowers, W.J., 2008. Detailed immunohistochemical characterization of temporal and spatial progression of Alzheimer's disease-related pathologies in male triple-transgenic mice. BMC Neurosci. 9, 81. https://doi.org/10.1186/1471-2202-9-81.
McKeith, I., Cummings, J., 2005. Behavioural changes and psychological symptoms in dementia disorders. Lancet Neurol. 4 (11), 735–742. https://doi.org/10.1016/S1474-4422(05)70219-2.
Mesholam, R.I., Moberg, P.J., Mahr, R.N., Doty, R.L., 1998. Olfaction in neurodegenerative disease: a meta-analysis of olfactory functioning in Alzheimer's and Parkinson's diseases. Arch. Neurol. 55 (1), 84–90.
Michelini, E.T., Flynn, G.C., 1999. The unique chaperone operon of Thermotoga maritima: cloning and initial characterization of a functional Hsp70 and small heat shock protein. J. Bacteriol. 181 (14), 4237–4244.
Minoshima, S., Giordani, B., Berent, S., Frey, K.A., Foster, N.L., Kuhl, D.E., 1997. Metabolic reduction in the posterior cingulate cortex in very early Alzheimer's disease. Ann. Neurol. 42 (1), 85–94. https://doi.org/10.1002/ana.410420114.
Mirrione, M.M., Schiffer, W.K., Fowler, J.S., Alexoff, D.L., Dewey, S.L., Tsirka, S.E., 2007.

A novel approach for imaging brain-behavior relationships in mice reveals unexpected metabolic patterns during seizures in the absence of tissue plasminogen activator. Neuroimage 38 (1), 34–42. https://doi.org/10.1016/j.neuroimage.2007.06.032.

Morbelli, S., Piccardo, A., Villavecchia, G., Dessi, B., Brugnolo, A., Piccini, A., ... Nobili, F., 2010. Mapping brain morphological and functional conversion patterns in amnestic MCI: a voxel-based MRI and FDG-PET study. Eur. J. Nucl. Med. Mol. Imaging 37 (1), 36–45. https://doi.org/10.1007/s00259-009-1218-6.

Mosconi, L., 2005. Brain glucose metabolism in the early and specific diagnosis of Alzheimer's disease. FDG-PET studies in MCI and AD. Eur. J. Nucl. Med. Mol. Imaging 32 (4), 486–510. https://doi.org/10.1007/s00259-005-1762-7.

Mosconi, L., Pupi, A., De Leon, M.J., 2008a. Brain glucose hypometabolism and oxidative stress in preclinical Alzheimer's disease. Ann. N. Y. Acad. Sci. 1147, 180–195. https://doi.org/10.1196/annals.1427.007.

Mosconi, L., Tsui, W.H., Herholz, K., Pupi, A., Drzezga, A., Lucignani, G., ... de Leon, M.J., 2008b. Multicenter standardized 18F-FDG PET diagnosis of mild cognitive impairment, Alzheimer's disease, and other dementias. J. Nucl. Med. 49 (3), 390–398. https://doi.org/10.2967/jnumed.107.045385.

Mutisya, E.M., Bowling, A.C., Beal, M.F., 1994. Cortical cytochrome oxidase activity is reduced in Alzheimer's disease. J. Neurochem. 63 (6), 2179–2184.

Naletova, I., Schmalhausen, E., Kharitonov, A., Katrukha, A., Saso, L., Caprioli, A., Muronetz, V., 2008. Non-native glyceraldehyde-3-phosphate dehydrogenase can be an intrinsic component of amyloid structures. Biochim. Biophys. Acta 1784 (12), 2052–2058. https://doi.org/10.1016/j.bbapap.2008.07.013.

Nestor, P.J., Fryer, T.D., Smielewski, P., Hodges, J.R., 2003. Limbic hypometabolism in Alzheimer's disease and mild cognitive impairment. Ann. Neurol. 54 (3), 343–351. https://doi.org/10.1002/ana.10669.

Nicholson, R.M., Kusne, Y., Nowak, L.A., LaFerla, F.M., Reiman, E.M., Valla, J., 2010. Regional cerebral glucose uptake in the 3xTG model of Alzheimer's disease highlights common regional vulnerability across AD mouse models. Brain Res. 1347, 179–185. https://doi.org/10.1016/j.brainres.2010.05.084.

Niwa, K., Kazama, K., Younkin, S.G., Carlson, G.A., Iadecola, C., 2002. Alterations in cerebral blood flow and glucose utilization in mice overexpressing the amyloid precursor protein. Neurobiol. Dis. 9 (1), 61–68. https://doi.org/10.1006/nbdi.2001.0460.

Oddo, S., Caccamo, A., Kitazawa, M., Tseng, B.P., LaFerla, F.M., 2003a. Amyloid deposition precedes tangle formation in a triple transgenic model of Alzheimer's disease. Neurobiol. Aging 24 (8), 1063–1070.

Oddo, S., Caccamo, A., Shepherd, J.D., Murphy, M.P., Golde, T.E., Kayed, R., ... LaFerla, F.M., 2003b. Triple-transgenic model of Alzheimer's disease with plaques and tangles: intracellular Abeta and synaptic dysfunction. Neuron 39 (3), 409–421.

Oddo, S., Caccamo, A., Smith, I.F., Green, K.N., LaFerla, F.M., 2006. A dynamic relationship between intracellular and extracellular pools of Abeta. Am. J. Pathol. 168 (1), 184–194.

Oh, K.J., Perez, S.E., Lagalwar, S., Vana, L., Binder, L., Mufson, E.J., 2010. Staging of Alzheimer's pathology in triple transgenic mice: a light and electron microscopic analysis. Int. J. Alzheimers Dis. 2010. https://doi.org/10.4061/2010/780102.

Oh, H., Madison, C., Baker, S., Rabinovici, G., Jagust, W., 2016. Dynamic relationships between age, amyloid-beta deposition, and glucose metabolism link to the regional vulnerability to Alzheimer's disease. Brain 139 (Pt 8), 2275–2289. https://doi.org/10.1093/brain/aww108.

Oyama, R., Yamamoto, H., Titani, K., 2000. Glutamine synthetase, hemoglobin alpha-chain, and macrophage migration inhibitory factor binding to amyloid beta-protein: their identification in rat brain by a novel affinity chromatography and in Alzheimer's disease brain by immunoprecipitation. Biochim. Biophys. Acta 1479 (1–2), 91–102.

Parihar, M.S., Brewer, G.J., 2007. Mitoenergetic failure in Alzheimer disease. Am. J. Physiol. Cell Physiol. 292 (1), C8–23. https://doi.org/10.1152/ajpcell.00232.2006.

Parker Jr., W.D., Filley, C.M., Parks, J.K., 1990. Cytochrome oxidase deficiency in Alzheimer's disease. Neurology 40 (8), 1302–1303.

Paxinos, G., Franklin, K.B.J., 2013. Paxinos and Franklin's the Mouse Brain in Stereotaxic Coordinates, 4th edition. .

Perneczky, R., Drzezga, A., Diehl-Schmid, J., Li, Y., Kurz, A., 2007. Gender differences in brain reserve : an (18)F-FDG PET study in Alzheimer's disease. J. Neurol. 254 (10), 1395–1400. https://doi.org/10.1007/s00415-007-0558-z.

Peters, J.M., Hummel, T., Kratzsch, T., Lotsch, J., Skarke, C., Frolich, L., 2003. Olfactory function in mild cognitive impairment and Alzheimer's disease: an investigation using psychophysical and electrophysiological techniques. Am. J. Psychiatry 160 (11), 1995–2002. https://doi.org/10.1176/appi.ajp.160.11.1995.

Petry, F.R., Pelletier, J., Bretteville, A., Morin, F., Calon, F., Hebert, S.S., ... Planel, E., 2014. Specificity of anti-tau antibodies when analyzing mice models of Alzheimer's disease: problems and solutions. PLoS One 9 (5), e94251. https://doi.org/10.1371/journal.pone.0094251.

Poisnel, G., Herard, A.S., El Tannir El Tayara, N., Bourrin, E., Volk, A., Kober, F., ... Dhenain, M., 2012. Increased regional cerebral glucose uptake in an APP/PS1 model of Alzheimer's disease. Neurobiol. Aging 33 (9), 1995–2005. https://doi.org/10.1016/j.neurobiolaging.2011.09.026.

Price, J.L., Ko, A.I., Wade, M.J., Tsou, S.K., McKeel, D.W., Morris, J.C., 2001. Neuron number in the entorhinal cortex and CA1 in preclinical Alzheimer disease. Arch. Neurol. 58 (9), 1395–1402.

Reiman, E.M., Uecker, A., Gonzalez-Lima, F., Minear, D., Chen, K., Callaway, N.L., ... Games, D., 2000. Tracking Alzheimer's disease in transgenic mice using fluorodeoxyglucose autoradiography. Neuroreport 11 (5), 987–991.

Reiman, E.M., Chen, K., Alexander, G.E., Caselli, R.J., Bandy, D., Osborne, D., ... Hardy, J., 2004. Functional brain abnormalities in young adults at genetic risk for late-onset Alzheimer's dementia. Proc. Natl. Acad. Sci. U. S. A. 101 (1), 284–289. https://doi.org/10.1073/pnas.2635903100.

Rojas, S., Herance, J.R., Gispert, J.D., Abad, S., Torrent, E., Jimenez, X., ... Sanfeliu, C., 2013. In vivo evaluation of amyloid deposition and brain glucose metabolism of 5XFAD mice using positron emission tomography. Neurobiol. Aging 34 (7), 1790–1798. https://doi.org/10.1016/j.neurobiolaging.2012.12.027.

Salmon, E., Collette, F., Degueldre, C., Lemaire, C., Franck, G., 2000. Voxel-based analysis of confounding effects of age and dementia severity on cerebral metabolism in Alzheimer's disease. Hum. Brain Mapp. 10 (1), 39–48.

Sancheti, H., Patil, I., Kanamori, K., Diaz Brinton, R., Zhang, W., Lin, A.L., Cadenas, E., 2014. Hypermetabolic state in the 7-month-old triple transgenic mouse model of Alzheimer's disease and the effect of lipoic acid: a 13C-NMR study. J. Cereb. Blood Flow Metab. 34 (11), 1749–1760. https://doi.org/10.1038/jcbfm.2014.137.

Schulze, H., Schuler, A., Stuber, D., Dobeli, H., Langen, H., Huber, G., 1993. Rat brain glyceraldehyde-3-phosphate dehydrogenase interacts with the recombinant cytoplasmic domain of Alzheimer's beta-amyloid precursor protein. J. Neurochem. 60 (5), 1915–1922.

Shokouhi, S., Claassen, D., Riddle, W., 2014. Imaging brain metabolism and pathology in Alzheimer's disease with positron emission tomography. J. Alzheimers Dis. Parkinsonism 4 (2). https://doi.org/10.4172/2161-0460.1000143.

Showers, M.J., Lauer, E.W., 1961. Somatovisceral motor patterns in the insula. J. Comp. Neurol. 117, 107–115.

Silverman, D.H., Small, G.W., Chang, C.Y., Lu, C.S., Kung De Aburto, M.A., Chen, W., ... Phelps, M.E., 2001. Positron emission tomography in evaluation of dementia: regional brain metabolism and long-term outcome. JAMA 286 (17), 2120–2127.

Skovronsky, D.M., Doms, R.W., Lee, V.M., 1998. Detection of a novel intraneuronal pool of insoluble amyloid beta protein that accumulates with time in culture. J. Cell Biol. 141 (4), 1031–1039.

Small, S.A., Duff, K., 2008. Linking Abeta and tau in late-onset Alzheimer's disease: a dual pathway hypothesis. Neuron 60 (4), 534–542. https://doi.org/10.1016/j.neuron.2008.11.007.

Snow, W.M., Dale, R., O'Brien-Moran, Z., Buist, R., Peirson, D., Martin, M., Albensi, B.C., 2017. In vivo detection of gray matter neuropathology in the 3xTg mouse model of Alzheimer's disease with diffusion tensor imaging. J. Alzheimers Dis. 58 (3), 841–853. https://doi.org/10.3233/JAD-170136.

Sokoloff, L., 1981. Relationships among local functional activity, energy metabolism, and blood flow in the central nervous system. Fed. Proc. 40 (8), 2311–2316.

Stortz, G., Thiessen, J.D., Bishop, D., Khan, M.S., Kozlowski, P., Retiere, F., ... Sossi, V., 2017. Performance of a PET insert for high resolution small animal PET/MR imaging at 7T. J. Nucl. Med. https://doi.org/10.2967/jnumed.116.187666.

Sunaga, K., Takahashi, H., Chuang, D.M., Ishitani, R., 1995. Glyceraldehyde-3-phosphate dehydrogenase is over-expressed during apoptotic death of neuronal cultures and is recognized by a monoclonal antibody against amyloid plaques from Alzheimer's brain. Neurosci. Lett. 200 (2), 133–136.

Suzuki, Y., Yamamoto, S., Umegaki, H., Onishi, J., Mogi, N., Fujishiro, H., Iguchi, A., 2004. Smell identification test as an indicator for cognitive impairment in Alzheimer's disease. Int. J. Geriatr. Psychiatry 19 (8), 727–733. https://doi.org/10.1002/gps.1161.

Tan, J., Town, T., Paris, D., Mori, T., Suo, Z., Crawford, F., ... Mullan, M., 1999. Microglial activation resulting from CD40-CD40L interaction after beta-amyloid stimulation. Science 286 (5448), 2352–2355.

Tan, J., Town, T., Crawford, F., Mori, T., DelleDonne, A., Crescentini, R., ... Mullan, M.J., 2002. Role of CD40 ligand in amyloidosis in transgenic Alzheimer's mice. Nat. Neurosci. 5 (12), 1288–1293. https://doi.org/10.1038/nn968.

Thiessen, J.D., Shams, E., Stortz, G., Schellenberg, G., Bishop, D., Khan, M.S., ... Goertzen, A.L., 2016. MR-compatibility of a high-resolution small animal PET insert operating inside a 7 T MRI. Phys. Med. Biol. 61 (22), 7934–7956. https://doi.org/10.1088/0031-9155/61/22/7934.

Trounce, I.A., Kim, Y.L., Jun, A.S., Wallace, D.C., 1996. Assessment of mitochondrial oxidative phosphorylation in patient muscle biopsies, lymphoblasts, and transmitochondrial cell lines. Methods Enzymol. 264, 484–509.

Ulrich, J., 1985. Alzheimer changes in nondemented patients younger than sixty-five: possible early stages of Alzheimer's disease and senile dementia of Alzheimer type. Ann. Neurol. 17 (3), 273–277. https://doi.org/10.1002/ana.410170309.

Valla, J., Berndt, J.D., Gonzalez-Lima, F., 2001. Energy hypometabolism in posterior cingulate cortex of Alzheimer's patients: superficial laminar cytochrome oxidase associated with disease duration. J. Neurosci. 21 (13), 4923–4930.

Valla, J., Schneider, L., & Reiman, E. M. (2006). Age- and transgene-related changes in regional cerebral metabolism in PSAPP mice. Brain Res., 1116(1), 194–200. doi: https://doi.org/10.1016/j.brainres.2006.07.097.

Valla, J., Gonzalez-Lima, F., Reiman, E.M., 2008. FDG autoradiography reveals developmental and pathological effects of mutant amyloid in PDAPP transgenic mice. Int. J. Dev. Neurosci. 26 (3–4), 253–258. https://doi.org/10.1016/j.ijdevneu.2008.02.003.

Verdier, Y., Huszar, E., Penke, B., Penke, Z., Woffendin, G., Scigelova, M., ... Janaky, T., 2005. Identification of synaptic plasma membrane proteins co-precipitated with fibrillar beta-amyloid peptide. J. Neurochem. 94 (3), 617–628. https://doi.org/10.1111/j.1471-4159.2005.03158.x.

Wang, J., Eslinger, P.J., Doty, R.L., Zimmerman, E.K., Grunfeld, R., Sun, X., ... Yang, Q.X., 2010. Olfactory deficit detected by fMRI in early Alzheimer's disease. Brain Res. 1357, 184–194. https://doi.org/10.1016/j.brainres.2010.08.018.

Weiner, H.L., Frenkel, D., 2006. Immunology and immunotherapy of Alzheimer's disease. Nat. Rev. Immunol. 6 (5), 404–416. https://doi.org/10.1038/nri1843.

Wu, Z., Yang, B., Liu, C., Liang, G., Eckenhoff, M.F., Liu, W., ... Wei, H., 2015. Long-term dantrolene treatment reduced intraneuronal amyloid in aged Alzheimer triple transgenic mice. Alzheimer Dis. Assoc. Disord. 29 (3), 184–191. https://doi.org/10.1097/WAD.0000000000000075.

Wyss-Coray, T., 2006. Inflammation in Alzheimer disease: driving force, bystander or

beneficial response? Nat. Med. 12 (9), 1005–1015. https://doi.org/10.1038/nm1484.

Zatorre, R.J., Jones-Gotman, M., Evans, A.C., Meyer, E., 1992. Functional localization and lateralization of human olfactory cortex. Nature 360 (6402), 339–340. https://doi.org/10.1038/360339a0.

Zhang, C., Wong-Riley, M.T., 2000. Synthesis and degradation of cytochrome oxidase subunit mRNAs in neurons: differential bigenomic regulation by neuronal activity. J. Neurosci. Res. 60 (3), 338–344. https://doi.org/10.1002/(SICI)1097-4547(20000501)60:3<338::AID-JNR8>3.0.CO;2-1.

Zhang, X., Stortz, G., Sossi, V., Thompson, C.J., Retiere, F., Kozlowski, P., ... Goertzen, A.L., 2013. Development and evaluation of a LOR-based image reconstruction with 3D system response modeling for a PET insert with dual-layer offset crystal design. Phys. Med. Biol. 58 (23), 8379–8399. https://doi.org/10.1088/0031-9155/58/23/8379.